Catena 254 (2025) 108908

Contents lists available at ScienceDirect

Catena

journal homepage: www.elsevier.com/locate/catena

Limits to fluvial planimetric adjustment imposed by anthropogenic confinement

Michael Vinicius de Sordi [a,*], Giovanni Vezzoli [b], Francesco Brardinoni [a,*]

[a] Department of Biological, Geological and Environmental Sciences, University of Bologna, Bologna, Italy
[b] Department of Earth and Environmental Sciences, University of Milano-Bicocca, Milano, Italy

ARTICLE INFO

Keywords:
Anthropogenic confinement
Geomorphic threshold
Planimetric adjustment
Secondary channels
Sensitivity to change
Sedimentary imbalance
Large rivers

ABSTRACT

The ability of a river to respond to sedimentary perturbations relates to the typology and degree of confinement, which dictates its potential for lateral migration. Over the past century, large rivers worldwide have become increasingly confined by rigid anthropogenic structures as a result of land reclamation and urbanization. However, owing to limited quantitative characterization of anthropogenic confinement, the inherent effects on fluvial adjustment have remained poorly constrained. In the Po River, Italy, historical anthropogenic changes are responsible for profound simplification of channel typology. These changes have left a fluvial mainstem dominantly bounded by levees, groins and similar structures that limit channel migration, thus lateral sediment supply. The planimetric evolution of the Po River mainstem is examined through multi-temporal (1954–2021) mapping of the active channel bed including the secondary channels. These variates are analyzed with respect to the concurrent degree of anthropogenic confinement across six valley segments. To quantify anthropogenic confinement, we map the active channel bed on six sequential airphoto sets and historical topographic maps, and then classify the relevant margins into natural (i.e., mobile) and artificial (i.e., immobile/confining) ones. This analysis reveals that: (i) anthropogenic confinement has increased across segments by a varying degree that ranges between 10 % and 21 %; (ii) that the current confinement increases downstream from 20 % to 61 %; and (iii) that a complex pattern of historical adjustment exists and is primarily controlled by confinement. Following mining collapse in the 1980 s, proximal segments S1-S3 with confinement < 33 % were able to adjust through widening (i.e., rebounding) and reactivation of secondary channels to conditions of increased sediment supply originating upstream and along the adjoining tributaries. Conversely, distal segments S4-S6 with confinement approaching a threshold of 45 % (and greater) have remained insensitive to such changes and continued to narrow, despite concurrent severe hydrological forcing. More locally, this lack of sensitivity is enhanced by the hydroelectric Isola Serafini complex, which today still forces some downstream bed degradation over about 40 km. At the (finer) reach scale, representing the rebound ratio (RR) – a dimensionless metric of planimetric recovery past the 1980 s historical low – as a function of confinement affords definition of a more robust threshold, which drops slightly to about 40 %, and enables to illuminate confluence and barrier effects. This work highlights the value of quantifying anthropogenic confinement, to complement current awareness on river fragmentation and barrier removal towards improved management solutions in the Anthropocene.

1. Introduction

Alluvial channels can respond to changes in sediment supply through gradation, that is, by adjusting their local characteristics – including gradient, geometry, morphology, or bed surface texture – at no excess capacity (e.g., Gilbert, 1914; Mackin, 1948; Leopold and Bull, 1979; Lisle, 1982; Madej, 2001; Cook et al., 2020). Beyond gradation, fluvial adjustment can involve significant change in alluvial storage associated with the vertical and lateral mobility of the bed (e.g., Hassan et al., 2007, 2024; Pryor et al., 2011; Luzi et al., 2021). In turn, the ability of an alluvial channel to adjust to sedimentary imbalance is conditioned, among other variables, by the typology and degree of confinement (e.g., Schumm, 1985; Kellerhals and Church, 1989; Fryirs et al., 2016), which dictates its potential to migrate sideways and to exchange (i.e., recruit or deposit) sediment with the adjacent floodplain (e.g., Dunne et al., 1998).

Over the last century – particularly after World War II – rivers across

* Corresponding authors.
E-mail addresses: michael.desordi@unibo.it (M.V. de Sordi), francesco.brardinoni@unibo.it (F. Brardinoni).

https://doi.org/10.1016/j.catena.2025.108908
Received 9 November 2024; Received in revised form 14 February 2025; Accepted 5 March 2025
Available online 14 March 2025

Europe have experienced widespread anthropogenic disturbance. On the one hand, fluvial corridors have served as sources of readily available raw material for construction works and consequently have undergone dramatic depletion in sediment storage (e.g., Belletti et al., 2016; Rascher et al., 2018; Parrinello et al., 2021). On the other hand, the implementation of engineering structures for flood protection, navigation, or hydropower production, have largely disconnected natural source-to-sink pathways, inducing sedimentary disequilibrium, as exemplified by channel pattern simplification, drastic active channel narrowing and widespread incision (e.g., Liébault and Piégay, 2001,2002; Surian and Rinaldi, 2003; Keesstra et al., 2005; Surian et al., 2009; Ollero, 2010; Comiti, 2012; Magdaleno et al., 2012; Latapie et al., 2014; Provansal et al., 2014; David et al., 2016; Mandarino et al., 2019; Ylla Arbós et al., 2021; Llena et al., 2024).

Concurrently, the geomorphic effects of similar human pressures have been masked by transient land cover conditions in upland tributary basins associated with farmland abandonment and natural reforestation, thus adding further complexity to the dynamics of sediment production on the slopes (e.g., Persichillo et al., 2017; Pittau et al., 2024), sediment delivery to streams (e.g., Persichillo et al., 2018), and in-channel routing (e.g., Liébault and Piégay, 2001; Scorpio and Piégay, 2021). As a result, causal linkages between specific sources of anthropogenic disturbance and the style and magnitude of fluvial adjustment remain largely elusive (Scorpio et al., 2024).

In this context of widespread and prolonged anthropogenic forcing, the Po River, the largest fluvial system of Italy, is no exception. Prior studies conducted on unconfined and partly confined reaches of its main tributaries, have constrained a three-phase conceptual model of planimetric adjustment involving: (i) moderate narrowing between the mid-19th century and the 1950 s; (ii) further and more intense narrowing between the 1950 s and the late 1980 s (or early 1990 s); and (iii) post-1990 s stability, or partial regain in active channel width, followed by

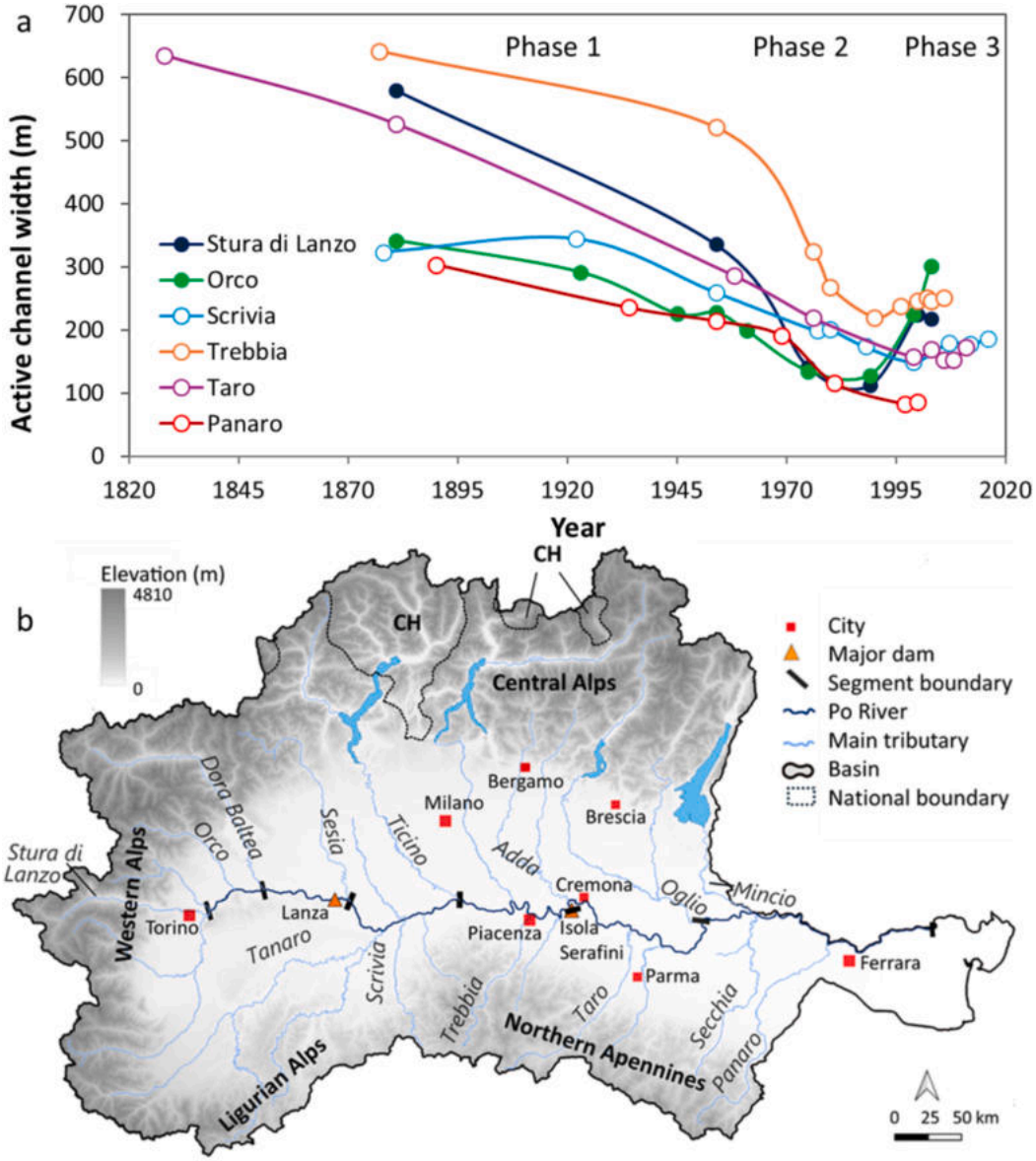

Fig. 1. (a) Historical planimetric adjustment in active channel width across selected tributaries of the Po River. See main text for explanation of the three phases of adjustment. (b) Simplified map of the Po River basin, including the main tributaries and the mainstem subdivided into six segments between the confluence with Stura di Lanzo River and the Po delta apex. Data shown refer to unconfined reaches in the main alluvial plain of: Stura di Lanzo River (reach length = 10.5 km) and Orco (reach length = 31 km) (from Pellegrini et al., 2008); Scrivia River (reach length = 40 km; from Mandarino et al., 2019); Trebbia River (reach length = 31 km; from Bollati et al., 2014); Taro River (reach length = 54 km; Clerici et al. 2015); Panaro River (reach length = 38 km; Rinaldi et al. 2010) (see Suppl. Table 1 for information on tributary basin size). In panel a, filled and empty symbols indicate tributaries originating respectively from the Alps and the Apennines.

second-order decadal fluctuations (Fig. 1a) (Surian and Rinaldi, 2003; Pellegrini et al., 2008; Surian et al., 2009; Rinaldi et al., 2010; Bollati et al., 2014; Clerici et al., 2015; Mandarino et al., 2019; Scorpio et al., 2024). These phases of narrowing, generally interpretated as a morphological response to decreased sediment supply and in-channel sediment storage, witnessed concurrent simplification in channel pattern (e.g., deactivation of secondary channels and reduction of sinuosity), as well as bed incision at reference channel cross sections.

By comparison, the historical adjustment of the entire Po River mainstem has received less attention, and consequently, it is unclear whether the same conceptual model of evolution constrained for the tributaries applies to a much larger and complex fluvial system. In this respect, the lack of a systematic characterization of confining artificial structures (such as levees and groins) has prevented the quantitative assessment of anthropogenic confinement. Equally important, existing quantitative studies on fluvial adjustment have focused either on selected unconfined reaches (e.g., Rinaldi, 2021; Nones et al., 2024) – to avoid possible confounding associated with varying degree of (natural or anthropogenic) confinement – or on heavily regulated counterparts, such as the channel reaches located upstream or downstream of the Isola Serafini Dam (e.g., Maselli et al., 2018; Brenna et al., 2024). Therefore, a comprehensive evaluation of channel adjustment at the mainstem scale in response to anthropogenic forcing, and artificial confinement in particular, is missing. This is a critical shortcoming that limits our understanding of perturbed fluvial systems, and most importantly hampers the implementation of efficient management strategies for recovering sedimentary balance and restoring the riverine ecological services of the Po River.

To address this gap, while wishing to disentangle (or rule out) the effects of multiple anthropogenic disturbances, this work addresses post-1950 channel adjustment of the Po River from its confluence with Stura di Lanzo River in Torino, down to the apex of the delta near Ferrara (Fig. 1b). Within these temporal and spatial boundaries, the specific objectives of this work aim: (i) to characterize the historical trend of anthropogenic confinement along the Po River mainstem; and therein (ii) to constrain possible causal linkages between the degree of anthropogenic confinement, including the location of major artificial barriers, and the historical trend of channel adjustment. Operationally, to pursue these objectives we subdivide the Po River into six morphological valley segments, map the relevant active channel bed over six sequential aerial photo sets (i.e., 1954–55; 1975–78; 1988–89; 1998–99; 2004–05; and 2021), classify the active channel margins into artificial and natural ones, and finally quantify the degree of anthropogenic confinement. In particular, exploiting a well-constrained, historical fluctuation in sediment supply associated with a one-order of magnitude rise and fall of in-channel mining (i.e., from the early 1970 s through the early 1980 s), and the occurrence of three of the largest channel-forming floods since 1950 (i.e., between 1994 and 2002; see Section 2), we examine the Po River mainstem planimetric adjustment to "post-mining conditions" as a function of anthropogenic confinement (Sections 3 and 4), and evaluate the effect of spatial resolution (Section 5).

2. Setting

The study area includes the 479.3 km portion of the Po River (basin area ~ 74,300 km^2), from the confluence with Stura di Lanzo River (200 m above sea level [asl]), in Torino, down to the apex of the river delta (−11 m asl) (Fig. 1b). The river originates from Mount Monviso (3841 m asl) and flows east for ~650 km before entering the Adriatic Sea, at the border between the Veneto and Emilia-Romagna regions of Italy. The northern and eastern divides are defined by the Central and Southern Alps, with tributaries draining mainly carbonate (limestone and dolostone), plutonic-volcanic and metamorphic rocks. The southern divides are constrained by the Ligurian Alps and Northern Apennines. The former are dominated by ophiolites, metasediments and flysch, and the latter are mainly underlain by sandstones, limestones, and mudstones.

Given its size, the climate across the Po River basin exhibits high spatial variability, from sub-continental (Alpine and Boreal) to Mediterranean (Warm Temperate) (Diodato et al., 2020). Along the river mainstem, mean annual precipitation varies from 881 mm in Torino (1954–2021, Arpa Piemonte, 2024) to 820 mm in Cremona (1954–2005, 2007–2021, Arpa Lombardia, 2024) and 635 mm in Ferrara (Arpae Emilia-Romagna, 2017; 2023). The annual flow regime is characterized by two low-water periods in winter and summer, and high flows in the late fall and the spring (Cattaneo et al., 2003). In this context, Alpine tributaries contribute maximum water flow during the snowmelt freshet in late spring (May–June), whereas water supply from the Apennines derive mostly from rainstorms of Atlantic origin in the spring (March-May) and the fall (October-November). Mean daily discharge (1954–2021) at Pontelagoscuro, near Ferrara, is approximately 1,400 m^3/s (Arpae Emilia-Romagna, 2021; 2023), with an estimated 10-year peak flow (T_{10}) of about 8,000 m^3/s (Marchi et al., 1995) (Fig. 2a).

Following the largest recorded drought experienced by the Po River in 2022, Montanari et al. (2023) identified a long-term declining trend in daily summer (i.e., June-July) discharge at Pontelagoscuro station. This seasonal decline, which appears to have become stronger and stronger in more recent decades, has been associated to local changes in hydrologic seasonality and water use, superimposed to the global trend of climate change. By contrast, when considering all seasons, although a general increase in daily streamflow statistics has been reported in the recent decades – chiefly attributed to the embankment works conducted along the Po River mainstem – no significant historical trend could be constrained (Zanchettin et al., 2008; Montanari, 2012; Domeneghetti et al., 2015). In particular, Domeneghetti et al. (2015) concluded that the likelihood of extreme flood events has not significantly changed over the past half a century.

Consistent with these findings, the 1954–2021 historical record of peak annual values of daily flows at Pontelagoscuro (Fig. 2a), as well as the mean (Suppl. Fig. 2a), and minimum counterparts (Suppl. Fig. 2b) show no statistically significant trend (i.e., Mann-Kendall (M−K) ρ-values at 0.05 confidence level), neither when considering separately the photographic time intervals used in this study (Suppl. Table 2). More qualitatively, the 1976–1979 and 1994–2002 period stand out for hosting large historical floods. The former is characterized by three of the top ten floods; the latter hosts three of the largest four floods occurred in the study period (i.e., 1994, 2000, and 2002). Between these two clusters, peak flows hardly exceed 6,000 m^3/s within a period of relatively consistent flows (Fig. 2a).

The alluvial plain of the Po River represents the foreland basin of the Alps and the Apennines linked to the collision of the Eurasian and African tectonic plates (Coward et al., 1989; Doglioni, 1993, Fantoni and Franciosi, 2010; Carminati and Doglioni, 2012). After the end of the Miocene Messinian salinity crisis, the Pliocene Po basin was a marine gulf separating the Alps from the Apennines. Since the Early Pleistocene, transition from marine to deltaic and finally fluvial sedimentation was progressively recorded from west to east. Especially, the onset of major glaciations (Muttoni et al., 2003) and the consequent increase in alluvial sediment supply led to a rapid progradation of the alluvial fans and the eastward advancement of deltaic systems (Garzanti et al., 2011; Scardia et al., 2012; Amadori et al., 2019).

Because of asymmetric distribution of subsidence and erosion rates (Livani et al., 2023) the Po plain can be subdivided into two sectors. A northern sector, where the subsurface sedimentary units fed from Alpine rivers are laterally extensive, tabular, and dominated by sand and gravel. A southern sector, where alluvial fans fed from the Apennines are embedded in clays and elongated in shape, reflecting abundance of mudrocks in the source areas, and greater rates of subsidence (Ori, 1993; Amorosi and Milli, 2001).

Today, the whole Pliocene – Quaternary sedimentary succession preserved in the basin is up to 8 km thick (Pieri and Groppi, 1981; Ghielmi et al., 2013) but the overall source-to-sink sediment cascade has been altered (and disconnected in places) by mining activity and by the

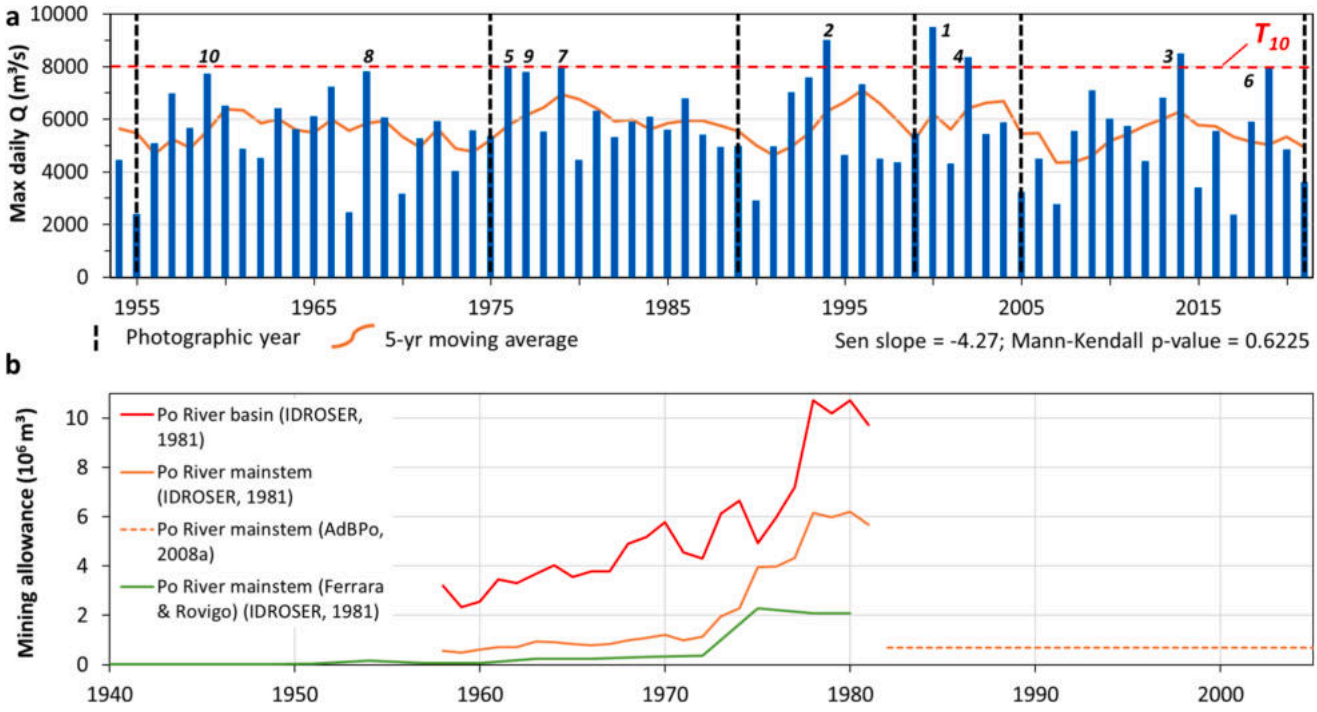

Fig. 2. (a) Maximum annual values of daily flow recorded at Pontelagoscuro (8 m asl) between 1 January 1954 and 31 December 2021. T_{10} (red line) refers to the 10-year recurrence discharge (i.e., 8,000 m^3/s) calculated for the 1918–1994 period (Marchi et al., 1995). Numbers 1 through 10 mark the ten highest peak flows, ranked from the largest (i.e., 1) in decreasing order, recorded in the 1954–2021 period. To ease visual interpretation, the relevant 5-year moving average is reported (i.e., red solid linework). The vertical dashed lines mark the photographic years used in this study. Note that the 1954–2021 trend of maximum daily discharges tested not significant to Mann-Kendall analysis at 0.05 level (Suppl. Table 2). (b) Volumetric sediment mining concessions allowed within the Po River basin (i.e., the mainstem and the tributaries) (1958–1981), and at in-channel sites along the Po River mainstem (1958–1981) and restricted to the channel reaches of the Rovigo and Ferrara provinces (1924–1981). The Rovigo and Ferrara provinces include the distalmost 90 km of the river mainstem, down to the apex of the Po delta (Suppl. Fig. 1). Mining concessions data sources: IDROSER (1981) and AdBPo (2008a).

emplacement of dams, (primary and secondary) levees, and bank stabilization works (e.g., Marchetti, 2002; Parrinello et al., 2021).

Although a comprehensive and quantitative historical picture detailing the spatial distribution of such engineering structures is missing, we know that most of the river training for navigation in the mid-to-distal portions of the mainstem i.e., between Cremona and the Secchia River confluence (Fig. 1b), entailing the installation of groins, was conducted in the 1930 s and 1940 s (Gorio, 1954). However, the entire training plan continued after World War II until the 1960 s, during which deactivation/regulation of secondary channels occurred (Galvani and Pellegrini, 2009). In this context, the Isola Serafini Dam (near Cremona) became operational in 1963 (AdBPo 2008a). The construction of this hydroelectric power plant – including the annexed navigation bypass – that diverts water past the turbines and across a 12-km meander, has drastically impacted river morpho-dynamics upstream. Through field observations and numerical modelling Maselli et al., (2018) concluded that river damming, by setting a higher baselevel and hampering sediment transfer, forced backwater flow dynamics, channel bar drowning and reduced lateral migration, particularly in the 30 kms located upstream of the dam.

After World War II, the Po River underwent additional anthropogenic disturbance due to intense and prolonged sand and gravel mining. Conservative estimates, based on official concessions, report that between 1958 and 1981 ~$53{\cdot}10^6$ m^3 and $131{\cdot}10^6$ m^3 of alluvium was extracted respectively from the bed of the study mainstem and over the entire river basin (IDROSER, 1981). Through time, concessions along the mainstem grew slowly from about $0.5{\cdot}10^6$ m^3 in the late 1950 s to about $1{\cdot}10^6$ m^3 in 1972, for then rising steeply until 1981 up to $6{\cdot}10^6$ m^3 (Fig. 2b). This historical pattern is mimicked by basin-wide concessions, as well as by those restricted to the riverbed located within the provinces of Rovigo and Ferrara (Suppl. Fig. 1). The latter data, which cover the distalmost 90 km of the river, are useful in that extend the historical record, attesting that concessions were relatively low since the 1920 s and remained low throughout the 1950 s (Fig. 2b) (IDROSER, 1981). From 1982 to 2005, annual rates of in-channel mining allowance were reduced, on average, by an order of magnitude (Fig. 2b), down to about 0.7 10^6 m^3 (AdBPo, 2008a).

This order of magnitude fluctuation in in-channel mining (i.e., from the early 1970 s to the early 1980 s), followed by three of the largest four floods (i.e., 1994, 2000 and 2002) recorded within the 1954–2021 study period, offers the opportunity to evaluate the sensitivity of the Po River mainstem to a well-constrained change in sediment supply across valley segments characterized by contrasting degrees of anthropogenic confinement.

3. Methods

The main objects of interest are the active channel bed, its width and the relevant degree of anthropogenic confinement. The active channel is the portion of a river comprised between the main margins (i.e., the banks) that includes the low-flow channel bed, as well as unvegetated to sparsely vegetated bars/islands and excludes vegetated bars/islands characterized by homogeneous forest (and/or shrub) cover (e.g., Leopold et al., 1964; Liébault and Piégay, 2002; Surian et al., 2009). In this work, we use the active channel width as a proxy of transport capacity in relation to in-channel sediment storage, as well as upstream and lateral sediment supply from the banks and the tributaries (e.g., Church, 2006; Bertrand and Liébault, 2019). Additionally, because wide channels generally evolve where there is a lot of lateral motion due to active bar deposition, we use the active channel width as a qualitative indicator of local sediment deposition (or the divergence of the sediment flux) (e.g., Llena et al., 2024).

3.1. Manual delineation and classification of the active channel margins

The multi-temporal mapping and characterization of the active channel bed is conducted primarily through visual inspection of six sets of sequential orthophoto mosaics (i.e., 1955, 1978, 1989, 1999, 2005 and 2021) (Table 1), and LIDAR-derived high resolution DTMs (i.e., 2004, 2005 and 2021) (Table 2), while drawing spatial information on fluvial terraces, alluvial fans, degree of channel incision and recent rates of bank retreat from the *Geomorphological Atlas of the Po River* (AdBPo, 2008b). Where available, the LiDAR DTMs are fused with underwater multibeam surveys. At complex sites, to improve appraisal of three-dimensional channel configuration and reduce mapping uncertainty, supplementary interpretation is conducted on channel cross sections extracted from the LiDAR-multibeam DTMs, and where available, from historical channel cross sections. Overall, mapped geomorphic elements include the two polylines of the active channel margins (i.e., one per each channel side), a corresponding polygon that encloses the active channel surface bounded by the two margins, and the relevant centerline (Fig. 3). Both the margin polylines and the active channel bed polygon are cut at right angles with the centerline using a regular spacing of 500 m.

Once the margins of the active channel are delineated, the degree of anthropogenic confinement for a given channel stretch is evaluated based on the topological intersection between the polygon of the active channel and the polylines of the possible confining structures (Fryirs et al., 2016; O'Brien et al., 2019). Specifically, the geomorphic elements needed for the evaluation of anthropogenic confinement in a given photo year include: (1) the polygons enclosing the extent of the active channel bed; and (2) the polylines associated with potentially confining features, such as the relevant man-made structures on the banks. To this end, the polylines forming the active channel margins are partitioned and classified into natural and artificial stretches, the latter being associated with man-made structures, including groins, longitudinal defense works (i.e., *defense works* for simplicity), and dikes. In the computation of the natural margins, the perimeter of the vegetated islands is not considered.

Basic, spatially distributed information on man-made structures confining the active channel is drawn from an existing vector database that includes historical data up to 2005 (AdBPo, 2006, 2008b, 2008c, 2008d). Owing to missing information on the year of construction and wishing to integrate multi-temporal information of planimetric channel geometry and man-made structure emplacement, we assign to each structure a minimum age, based on their first appearance on the historical topographic maps (i.e., 1954, 1979, 1990, 1995, and 1996) closest to the photo year of interest (Table 3) and on the orthophoto mosaics, and based on cartographic information contained in the *Po River Geomorphological Map* (NIER/CER, 1982) (i.e., it reports the structures built before 1982). During this procedure, missing structures in the existing database are manually digitized and added to the vector layer of the relevant photo year. For photo year 2021 (i.e., beyond the time span of the existing database) the updating of the artificial margins is conducted through manual mapping of new structures reported on 2021 topographic maps. This activity is complemented by visual examination of the 2021 orthophoto mosaic and the topographic cross sections extracted from the 2021 LiDAR DTM.

Table 1
Historical optical imagery used for the multi-temporal delineation and classification of the active channel bed and the relevant margins.

Photo Year	Nominal scale	Pixel size (m)	Bands	Source
1954–55	1:33.000	0.7 – 1.4	BW	RP[a], WMS LB[b], WMS E-R[c]
1975–78	1:5.000 – 1:15.000	0.3 – 1.4	BW, RGB	RP[a], WMS LB[b], WMS E-R[c]
1988–89	1:10.000	1	BW	WMS GN[d]
1998–99	1:10.000	1	RGB	WMS GN[d]
2004	1:2.000	0.2	RGB	AdBPo[e]
2005	1:2.000	0.2	RGB	AdBPo[e]
2021	1:2.000	0.15	RGB	AdBPo[e]

[a] Regione Piemonte.
[b] Geoportale Regione Lombardia https://www.geoportale.regione.lombardia.it.
[c] Geoportale Regione Emilia-Romagna: https://geoportale.regione.emilia-romagna.it.
[d] Geoportale Nazionale: https://www.pcn.minambiente.it.
[e] AdBPo – Autorità distrettuale di Bacino del Fiume Po.

The spatial distribution of natural and artificial margins through time is further consolidated based on the stability (or the planimetric channel changes) observed in the geometry of the mapped active channel bed between sequential photo years (Table 1). Given that the integrity of in-channel structures varies over time depending on their age, the level of maintenance and the history of hydrological forcing, the structures mapped and classified on the previous photographic year are retained only when the geometry of the artificial margins remains unchanged; vice versa, they are reclassified as natural. Overall, the combined database contains six layers (i.e., one per each photo year) in which the active channel margins are classified into natural and artificial, and each artificial stretch is further classified by structure type (i.e., groins, defense works and dikes).

Operationally, in this work the degree of confinement (C, expressed as percentage) for a given channel stretch s, is calculated according to Eq. (1), that is, as the ratio between the sum of the length of the artificial margins ($\sum L_{am}$) and the total length of the margins ($\sum L_s$):

$$C_s = \left(\sum L_{am} / \sum L_s\right) * 100 \quad (1)$$

Based on this formulation, an unconfined channel stretch characterized by natural margins (green linework in Fig. 3a), following urban and/or agricultural development may become increasingly confined due to the implementation of bank protection works (red linework), including the deactivation of secondary channels (Fig. 3b). Subsequently, this trend of increasing historical confinement may be reversed by progressive structural deterioration and/or sudden channel changes induced by a large flood. Similar dynamics may lead to the reactivation of natural secondary channels and/or the increase in planform sinuosity, which in both instances would imply a decrease in artificial confinement (Fig. 3c).

As schematically shown in Fig. 3, anthropogenic confinement can increase or decrease through time for multiple reasons. Here we provide a set of practical examples drawn from the Po River (Suppl. Fig. 3). An increase in confinement may derive from: (i) the construction of new longitudinal defense works, groins or dikes (Suppl. Fig. 13); (ii) the deactivation of secondary channels, with associated increase in planform sinuosity of the outer channel margins (Suppl. Fig. 1a and 1b); (iii) lateral migration through erosion of natural margins up to the base of existing levees, which become the "new" artificial margins (Suppl. Fig. 1c and 1d); (iv) the rectification of natural margins, resulting in sinuosity reduction, and thus leading to a decrease in the combined length of natural margins.

By contrast, a reduction in anthropogenic confinement may stem from: (i) the increase of planform sinuosity due to lateral migration, leading to an increase of the combined length of natural margins (Suppl. Fig. 3e and 3f); (ii) the dislocation or failure of defense works, groins or dikes due to migration dynamics leading to structural undercutting (Suppl. Fig. 3g and 3h); (iii) the reactivation of old secondary channels, or the formation of new ones with associated increase in planform sinuosity of the outer channel margins.

3.2. Active channel width and secondary channels

The active channel width for a given 500-m stretch "s" (W_s) is calculated according to Eq. (2), that is, by dividing the area of the active channel polygon (A_s) – from which vegetated bars/islands are excluded

Table 2
Gridded subaerial and submerged digital topography used in this study.

Year	Survey type	Grid size (m)	Vertical error (m)	Topography	Spatial coverage	Source
2004	LiDAR	2	0.2	subaerial	Pellice R. to Ticino R.	AdBPo[a]
2005	LiDAR & Multibeam	2	0.2 & 0.5	subaerial & submerged	Ticino R. to Po delta	AdBPo[a]
2021	LiDAR	1	0.08	subaerial	S. di Lanzo R. to Po delta	AdBPo
2021	Multibeam	1	0.5	submerged	Isola Serafini to Mincio R.	AdBPo

[a] https://www.adbpo.it/download/dtm_po_2004_2005/.

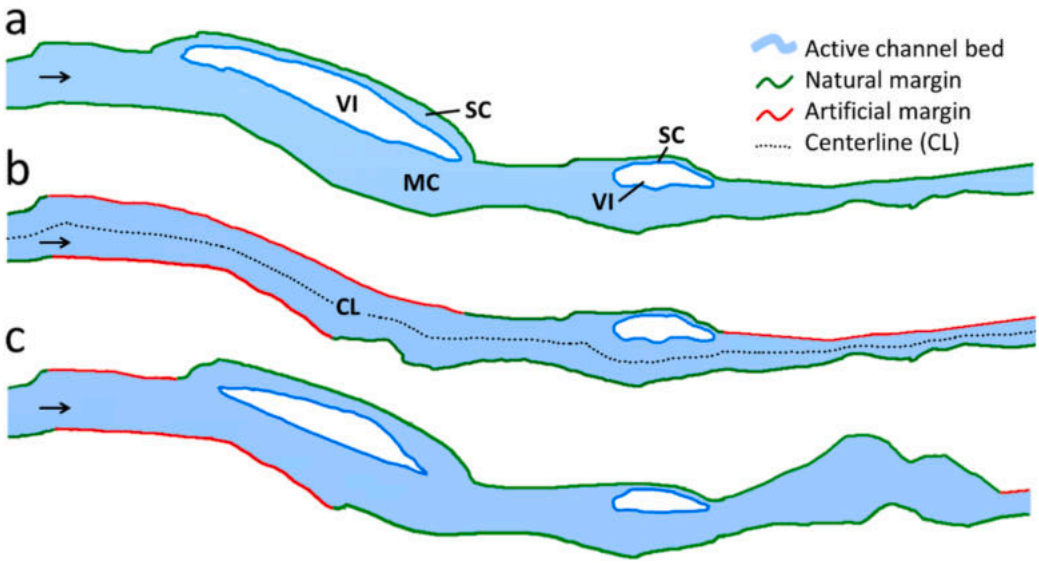

Fig. 3. Schematic evolution of a natural channel stretch undergoing increasing anthropogenic confinement, followed by deterioration of protection works: (a) initial planform configuration with natural margins; (b) margins become increasingly artificial through installation of protection and/or navigation works with concurrent deactivation of a secondary channel and the overall simplification of the channel pattern, including the reduction in planform sinuosity; and (c) with time, or owing to an exceptional flood, some protection structures become obliterated, and planform configuration regains complexity through formation of secondary channels and increase of sinuosity following lateral migration. Note that the margins of vegetated islands are not considered in the evaluation of confinement. MC = main channel; SC = secondary channel; CL = centerline; VI = vegetated island.

Table 3
Reference cartographic information used to build the database of anthropogenic structures in each photo year.

Photo year	Reference topographic map (WMS)	Nominal scale	Reference orthophoto[a]	Additional references
1955	1954–55	1:10,000	1954–55	MagisPo, 1954
1978	1979	1:10,000	1975–1978	MagisPo, 1979
1989	1990	1:10,000	1988–89	NIER/CER, 1982
1999	1995	1:10,000	1998–99	Topographic map 1996: 1:50,000 WMS
2005	–	–	2004–05	DTM 2004–05 AdBPo vector database (2006, 2008b,c,d)
2021	2021	1:10,000	2021	DTM 2021

[b]NIER/CER, 1982. Indagine fotointerpretativa dell'alveo del Fiume Po dalla confluenza del Tanaro a Pontelagoscuro. Studio Geologico GEOMAP di Firenze.
[a] See Table 1 for details.

– by the length of the relevant centerline (L_{Cs}) (Fig. 3b):

$$W_s = A_s/Lc_s \quad (2)$$

Besides cutting the Po River main stem into 500-m stretches, to control for the effects of local anomalies associated with discrete water and sediment inputs (e.g., tributary confluences) and barriers (e.g., dams) that may confound underlying spatial patterns of channel adjustment, we subdivide the Po River into six segments (Frissell et al., 1986; Montgomery e Buffington, 1997). This segmentation is based on the location of main confluences, dominant channel bed texture (gravel or sand), channel width, slope, degree of anthropogenic confinement as evaluated in photo year 2021, and presence/typology of secondary channels. In particular, the segments' upper ends were set: (1) upstream of major tributary confluences (i.e., Stura di Lanzo in segment S1, Dora Baltea in S2, Sesia in S3, Ticino in S4 and Oglio in S6); (2) at major dams (i.e., Isola Serafini in S5) (Fig. 1b). The lower end of segment 6, i.e., the downstream limit of the study area is defined at the Po River delta. This morphological approach seeks to reduce in-segment heterogeneity while maximizing between-segment differences, so that channel adjustment may be evaluated in relation to different channel typology (Church, 2006; Llena et al., 2024). In this work, subdivision into six segments wishes also to simplify graphical representation of the Po River evolution in time and space, while characterizing within-segment variability through statistical analysis of the 500-m channel stretches.

To evaluate the extent to which anthropogenic confinement can hamper the ability of a channel segment to respond to the order of magnitude increase in sediment supply (i.e., associated with the drastic reduction of in-channel mining concessions since 1981) through planimetric widening, we represent the so-called "rebound ratio" (RR) – the ratio between the active channel width at the peak of planimetric re-widening (ACW_{RE}; i.e., post-mining phase of recovery) (e.g., 2005) and the antecedent minimum active channel width (ACW_{SC}; i.e., culmination of sediment starved conditions)(e.g., 1989) (Eq. (3) – as a function of anthropogenic confinement in 1975–78, when mining was about to collapse:

$$RR = \text{median}\,ACW_{RE}/\text{median}\,ACW_{SC} \quad (3)$$

Accordingly, RR > 1.1 indicates a regain in active channel width > 10 %, whereas RR < 1 indicates no rebound to a larger channel configuration, but a tendency to planimetric narrowing.

To better constrain the sources of planform channel adjustment in relation to varying degree of anthropogenic conditioning beyond lateral confinement, we subdivide the active channel bed into main and secondary channel polygons, with the latter further classified into natural and regulated secondary channels. In this context, a decline in the number and area of natural secondary channels – in favor of regulated counterparts – would be regarded as a sign of decreasing in-channel sediment supply (or alluvial sediment storage) and concurrent loss of natural conditions (i.e., transition from wandering to single-thread channel pattern). In our historical analysis, to account for varying segment length and segment footprint area, the number and area of secondary channels are standardized respectively by segment length (#/km) and segment active channel area (ha/km^2).

3.3. Channel bed texture

Characterization of channel bed texture along the river mainstem relies on field sampling and lab sieving conducted between 2005 and 2006 (AdBPo, 2006; 2008c; 2008d). Data collection involved the bulk sampling of sand (about 2 kg each) and gravel (about 16 kg each) sediments at 173 sites from active fluvial bars. Selection of the sampling sites was dictated by ease of logistical access, as well as considering the occurrence of barriers (i.e., dams) and potential main sediment sources, such as tributary confluences. On the fluvial bars, a square frame with sides of 15 cm for sandy samples and 30 cm for gravel samples was positioned on a sedimentary homogeneous area. Sampling was conducted after manual removal of the surficial layer (i.e., 5-cm and 10-cm thick for sand and gravel surfaces, respectively) utilizing a spatula or a shovel. The samples were then subjected to granulometric analysis through mechanical sieving using also riffle box and splitter. Pebbles larger than 25 mm were measured individually using a digital reading caliper.

4. Results

To pursue the paper's objectives, we begin by introducing the six channel segments' characteristics in 2004–05 (Section 4.1). This snapshot was selected as it relies on the most complete set of topographic and photographic data, information on channel bed texture, as well as on original, vector-based, spatially distributed information of anthropogenic structures around the active channel. Subsequently, we track between 1955 and 2021 the historical evolution of the anthropogenic confinement, the number and area of secondary channels, and the active channel width. Specifically, we first illustrate these historical changes at the combined scale of the entire Po River mainstem (Section 4.2), and then across the single channel segments (Section 4.3). Further, we increase the spatial resolution of investigation by reporting local morphological examples to illustrate characteristic styles of morphological adjustment and bed level changes at reference channel cross sections (Section 4.4). Finally, to try explaining the anomalous planimetric adjustment in segment S5, exploiting existing repeat high-resolution topographic surveys, we examine the 2005–2021 sediment budget across selected reaches downstream of the Isola Serafini navigation bypass (Section 4.5).

4.1. Characteristics of the channel segments in 2004–05

The Po River mainstem shows a channel typology that varies from transitional ("Trans" for brevity in Table 4) across the three headmost segments, to dominantly single-thread further downstream. Travelling in the downstream direction, median slope gradient decreases from 0.3 m/km (S1) to 0.1 m/km (S6). As slope decreases and drainage area increases, channel bed texture becomes finer. Indeed, dominant bed texture varies from gravel (as coarse as coarse pebble) to sand and very fine sand, with channel bar median D50 dropping from 15 mm in segment S1 to 0.35 mm in segment S6 (Table 4). Interestingly, a major gravel-sand transition is found near the Ticino River confluence, as testified by the abrupt drop in the median D50 between segments S3 and S4 (Fig. 4). The transitional nature in channel bed texture of these two segments is also supported by the high spread of the D50 interquartile range that characterizes both S3 and S4. Further downstream, channel bed texture in S5 and S6 becomes increasingly enriched in finer fractions.

The downstream pattern of the active channel width is more complex. Median segment width increases from about 221 m in S1 and 228 m in S2 to 423 m in S3, but then declines progressively to 388 m in S4 and 353 m in S5, and finally peaks to 439 m in S6 (Table 4). As will be discussed later, this complexity may have to do with the varying degree of anthropogenic confinement, which exhibits a high degree of downstream variability. Accordingly, confinement is lowest in S1 (31 %) and S3 (37 %), increases to about 50 % in S2 and S4, and grows highest in S5 (58 %) and S6 (61 %).

Proximal segments S2 and S3 are also characterized by a natural component of confinement exerted by hillslopes. In S2, the total length of natural channel margins confined by hillslopes is 5.5 km and impart

Table 4
Summary characteristics of the study segments in year 2005. D_{50} values refer to sampling conducted on channel bars by AdBPo between 2005 and 2006 (AdBPo, 2006; 2008c; 2008d).

	Length (km)	Drain Area (km^2)	Bed material (bar D_{50}; n) [a]	Channel type	Median width (m)	Median slope (m/km)	AnCf (%) [b]	Groins [c] (m/km)	Secondary ch. [d] No.	Secondary ch. [d] Area (ha)
S1	32.2	9182	Gravel (15 mm; 9)	Single-thread	228	1.3	31	3	2 (1)	30 (11)
S2	48.7	13,718	Gravel (17 mm; 9)	Trans	221	1.1	52	0	6 (0)	58 (0)
S3	69.3	31,080	Gravel (10 mm; 26)	Trans	423	0.4	37	10	11 (0)	60 (0)
S4	87.0	42,708	Sand (0.60 mm; 21)	Single-thread	388	0.2	53	21	5 (6)	60 (30)
S5	103.7	56,780	Sand & finer (0.47 mm; 66)	Trans	351	0.2	58	439	2 (22)	26 (531)
S6	138.4	71,526	Sand & finer (0.35 mm; 42)	Single-thread	439	0.1	61	129	7 (10)	48 (209)

[a] Median D50; n = number of samples.
[b] Anthropogenic confinement.
[c] Linear meters of groins per kilometer of active channel.
[d] Number and combined area of natural and regulated (values in brackets) secondary channels.

c. Linear meters of groins per kilometer of active channel.
d. Number and combined area of natural and regulated (values in brackets) secondary channels.

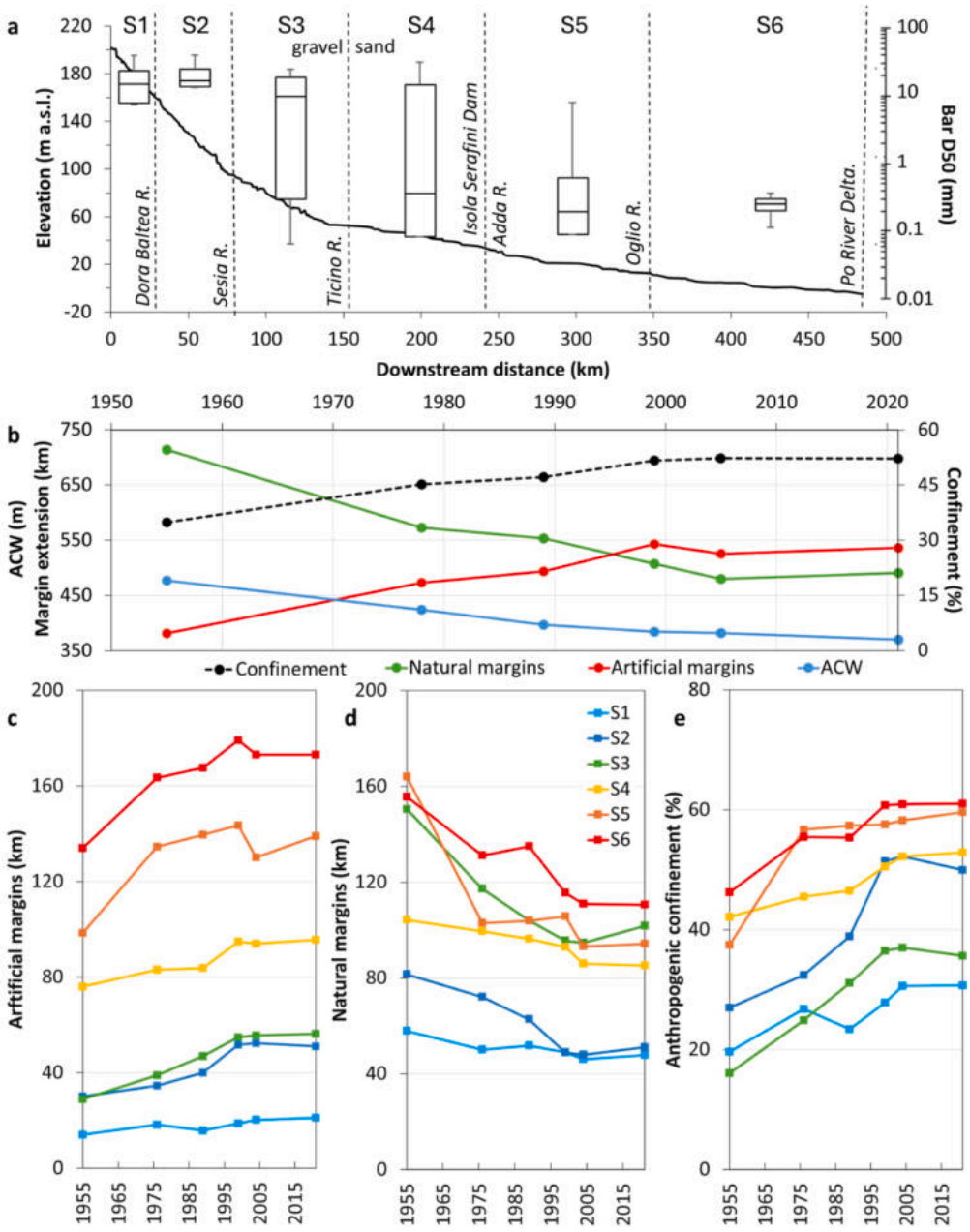

Fig. 4. (a) Long profile of the Po River mainstem between the Stura di Lanzo River confluence (upstream end of segment S1) and the apex of the Delta (downstream end of segment S6). Box plots report the distributions of the D_{50} from samples taken on the bars within each segment. Horizontal lines within the boxes indicate median D_{50} values, boxes enclose interquartile ranges (25–75%), whiskers indicate 10th and 90th percentiles. Note approximate location of the gravel-sand transition. Data source of grain size distributions: AdBPo (2006, 2008c, 2008d). (b) Mainstem-wide historical evolution of the length of artificial (red) and natural margins (green), and the relevant degree of anthropogenic confinement (black dashed line). Historical evolution (1954–2021) across the six Po River study segments of: (c) the length of the artificial margins; (d) the length of the natural margins; and (e) the degree of anthropogenic confinement.

an increase of 5.4 % to the segment's overall degree of confinement. In S3, naturally confined margins amount to 1.0 km only, which accounts for just an extra 0.5 % of confinement. Both regulated secondary channels and groins, indicators of artificial conditioning per se, are especially densely distributed within segment S5 and secondarily in S6 (Table 4).

4.2. *Mainstem-scale anthropogenic confinement and planimetric channel adjustment*

The combined length of the artificial margins around the active channel bed increases consistently through time, from 382 km in 1955 to 543 km in 1999 (Fig. 4b), for a total gain of 161 km. Subsequently, a sharp temporary drop in 2005 – likely associated with the largest peak flow recorded since 1950 (Fig. 2b), which brought about widespread bank erosion and structural damage – is followed by a partial regain until 2021. This historical trend is mirrored by a concurrent decline of

the natural margins' combined length, which drops by 234 km between 1955 and 2005 (i.e., from 714 km to 480 km), and then rebounds slightly in 2021 (Fig. 4b). The foregoing historical variability in the combined length of natural and artificial margins leads to a degree of anthropogenic confinement that increases progressively from 35 % in 1954 to 52 % in 1999, and then remains substantially constant. The median active channel width (ACW) decreases progressively by more than 100 m, from 477 m in 1955 to 370 m in 2021, except for the 1999–2005 period, during which it stays stable (Fig. 4b).

In agreement with an historical increase in anthropogenic confinement, the number and the combined area of natural channels decline between 1955 and 1989, whereas regulated counterparts increase (Suppl. Fig. 4). Natural secondary channels, here regarded as morphological indicators of fluvial wellbeing, hit an historical low (both in number and area) about a decade earlier than the peak previously observed in the combined length of the artificial margins. After 1989, their number increases, whereas the combined area remains about the same. The historical trend of regulated secondary channels differs, in that their number and combined area declines progressively through 2021 (Suppl. Fig. 4).

4.3. Variability across the channel segments

4.3.1. Anthropogenic confinement and planimetric adjustment

Subdivision of the Po River mainstem into six channel segments allows depicting a composite downstream pattern of historical changes with respect to the length of artificial and natural margins, the resulting degree of anthropogenic confinement (Fig. 4c–e), and the (median) active channel width (Fig. 5).

The historical evolution of the artificial margins across segments reveals that their length in 1955, and their growth through time, increase as one moves downstream (Fig. 4c). This increase, in absolute

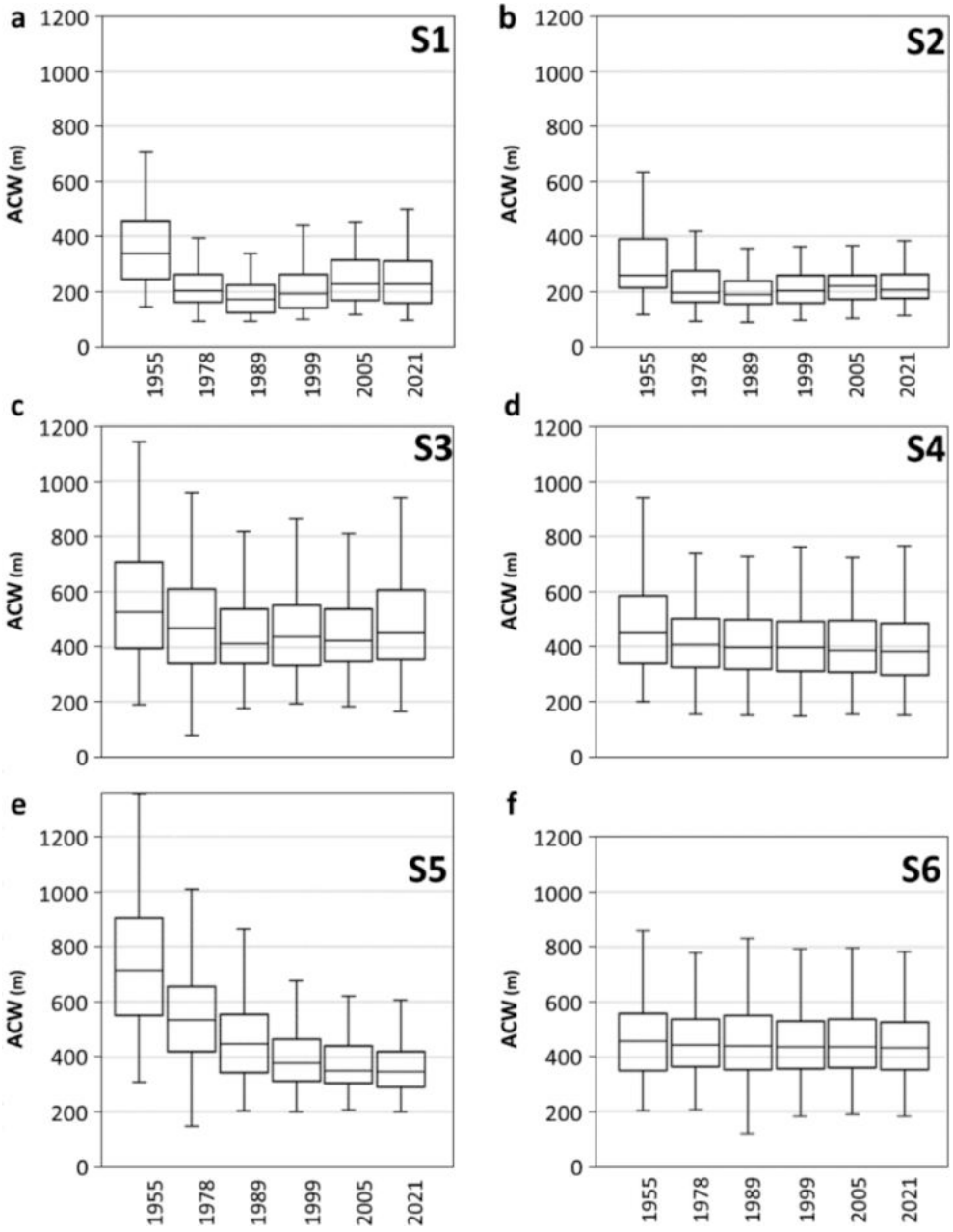

Fig. 5. Boxplots showing the historical (1955–2021) frequency distribution of the active channel width (ACW) measured across 500-m channel stretches: (a) S1; (b) S2; (c) S3; (d) S4; (e) S5; and (f) S6. Horizontal lines indicate median values, boxes enclose interquartile ranges, and whisker indicate 10th and 90th percentiles.

terms, is lowest in S1 (from 14 km to 21 km), and greatest in S5 (from 99 km to 139 km) and S6 (from 134 km to 173 km). In this context, the abrupt drop observed in 2005 is interpreted as the effect of the highest peak flow occurred in year 2000, which caused widespread damage to man-made structures in S5 and S6 (Fig. 4c). As expected, the historical growth in artificial margins is paralleled by a decrease of the natural counterparts. This decline, however, manifests as a set of more complex trends across the different segments (Fig. 4d), suggesting that what we are seeing may not be the effect of just a mere natural-to-artificial margin replacement. Overall, the historical shrinkage of the natural margins is lowest in S1 (10 km) and largest in S5 (70 km).

In broad agreement with the historical trend of the artificial margins, tracking anthropogenic confinement across the channel segments shows generalized increase between 1955 and 1999, followed by substantial stability – except in S2, where a decline occurs between 2005 and 2021 (Fig. 4e). This increase ranges from as little as 10 % in S4 (from 42 % in 1955 to 52 % in 2021) up to a maximum of 23 % in S2 (from 27 % to 50 % in 2021). Collectively, the historical changes in margin typology across the six study segments led to a spatial distribution of confinement in 2021 that increases progressively downstream: from 30 % in S1 to 61 % in S6.

Similarly to the anthropogenic confinement, the historical trend in active channel width (ACW) displays high variability across segments (Fig. 5). This is not surprising, considering that margin typology affects alluvial sediment supply (from the banks) and lateral mobility potential.

After a common 1955–1978 narrowing trend, albeit characterized by different magnitudes, historical ACW adjustment differ among segments. Proceeding in the downstream direction, gravel-bed segments S1 and S2, which score lowest and third lowest in 1955–89 anthropogenic confinement, continue to narrow until 1989 (i.e., median ACW drops from 339 m to 173 m in S1 and from 259 to 191 in S2), recover to partly wider configurations (at least) until 2005, and remain about stable thereafter (Fig. 5a and b).

ACW adjustment in gravel-bed segment S3 differs from S1 and S2 in that, median width reduction across the 1955–89 period is followed by over two decades of substantial stability, until a rewidening is observed between 2005 and 2021. Interestingly, the ACW frequency distributions in 1978 and 2021 are very similar, suggesting that some degree of recovery was achieved, at least in planimetric terms (Fig. 5c).

Segments S6 and S4, which score respectively highest and third highest in anthropogenic confinement, exhibit post-1978 planimetric adjustments characterized by stability and subtle narrowing, with no hint of width recovery. In S4, median ACW declines from 410 m in 1978 to 385 m in 2021 (Fig. 5d). In S6, the reduction is even lower: from 455 m in 1955 to 430 m in 2021 (Fig. 5f).

In contrast with the two adjacent segments, S5, which starts at Isola Serafini Dam, is characterized by a continuous and intense narrowing trend. Narrowing is particularly strong until 2005 (i.e., median ACW drops from 713 m to 351 m) and continues at slower pace thereafter (Fig. 5e).

Wishing to look for a possible underlying dependence of planimetric adjustment on confinement, we ran the (nonparametric) Spearman's rank correlation testing between median active channel width – standardized by drainage area to remove the systematic bias associated with the location of the different study segments along the Po River mainstem – and the contingent degree of confinement. Results show that indeed a strong inverse relation exists between these two variates (i.e., $n = 34$; coefficient = -0.89; p-value < 0.001).

With respect to the rebound ratio (RR) (see Section 3.2), this metric scores highest in S1 (1.32), intermediate in S2 (1.16), and lowest in S3 (1.09), whereas the highly confined S4 (0.97), S5 (0.79) and S6 (0.99) do not exhibit any recovery to wider channel configuration. Although not significant at the 0.05 level, given the limited number of observations, Spearman's rank correlation confirms that RR and confinement across the six study segments are inversely related (i.e., $n = 6$; coefficient = -0.771; p-value = 0.072).

4.3.2. Secondary channels

Conceptually, information on natural secondary channels should complement and corroborate prior evidence gathered from the historical adjustment of active channel width. For example, as much as a decreasing ACW through time is expected to reflect sediment starved conditions, a decline in natural secondary channels implies a transition from multi- to single-thread channel types, which in turn indicates a reduction in sediment supply and/or in-channel storage (Schumm, 1977; Church, 2006).

The number and combined area of natural secondary channels through time, standardized respectively by the relevant segment length and active channel footprint, vary substantially across the six study segments (Fig. 6). Between 1955 and 1978, a reduction in the number of natural secondary channels is observed, except in S4, which displays small historical fluctuations for the entire study period (Fig. 6a). Subsequently, diverging trends are apparent. In S1, the drop in natural secondary channels continues until 1998, after which, a significant regain in number occurs by 2021. In S2, the minimum value reached in 1998 remains about the same until 2021. In S3, a sharp rebound between 1998 and 2005 leads to natural secondary channels count comparable with the pre-1989 configuration. Although to a lesser extent, a symmetrical rebound in the number of natural secondary channels characterizes also segment S6, following the historical low reached in 1989. Segment S5, which incidentally experienced the highest increase in confinement and the most severe narrowing through time, stands out in that all natural secondary channels have disappeared by 2021 (Fig. 6a).

The historical decline in terms of natural secondary channels' combined area is even more evident (i.e., less noisy) and occurs mostly between 1955 and 1989 (Fig. 6b). Subsequently, the combined area remains consistently well below 0.1 ha/km^2, although some areal regain is observed in S1, S3 and S6 – coherently with observations made in terms of natural channel count (Fig. 6b).

The spatial and temporal evolution of regulated secondary channels is comparably much simpler. Their significance is very limited in space and time across segments S1, S2 and S3. Indeed, regulated channels cluster in segment S5 (downstream of the Isola Serafini Dam), and to a lesser extent in S6 (Fig. 6c and d). In S5, their number peaks in 1989 and then declines progressively until a minimum < 0.2 #/km is observed in 2021. By contrast, both S4 and S6 witness a moderate growth in regulated, with peaks reached respectively in 2005 and in 1998 throughout 2021 (Fig. 6b). The combined area per unit segment footprint confirms the significance of regulated secondary channels in segment S5, and secondarily in S6, with historical trends mimicking closely those just described in terms of count (Fig. 6d).

In this context, Spearman's rank correlation supports that the standardized number of natural and regulated secondary channel is inversely (i.e., $n = 36$; coefficient = -0.73; p-value < 0.001) and directly related with anthropogenic confinement (i.e., $n = 36$; coefficient = 0.59; p-value < 0.001). When considering the standardized area, the foregoing inverse (i.e., $n = 36$; coefficient = -0.68; p-value < 0.001), and direct (i.e., $n = 36$; coefficient = 0.57; p-value < 0.001) remain significant at the 0.01 level.

4.4. Local examples of historical adjustment and bed-level change

Downscaling the analysis of historical adjustment to 5-km channel stretches allows improving our understanding of the segment-wide planimetric tendencies shown above. On the one hand, this approach enables us to use information on bed-level changes (i.e., 1955/1975–2004/2021) at reference channel cross sections, and therefore to link planimetric and vertical channel changes. On the other hand, it permits to illustrate at a more meaningful geomorphic spatial resolution the effects of varying anthropogenic confinement on morphological adjustment, and therefore – since the abundance of (vegetated and unvegetated) bars, the degree of sinuosity and the presence of (natural

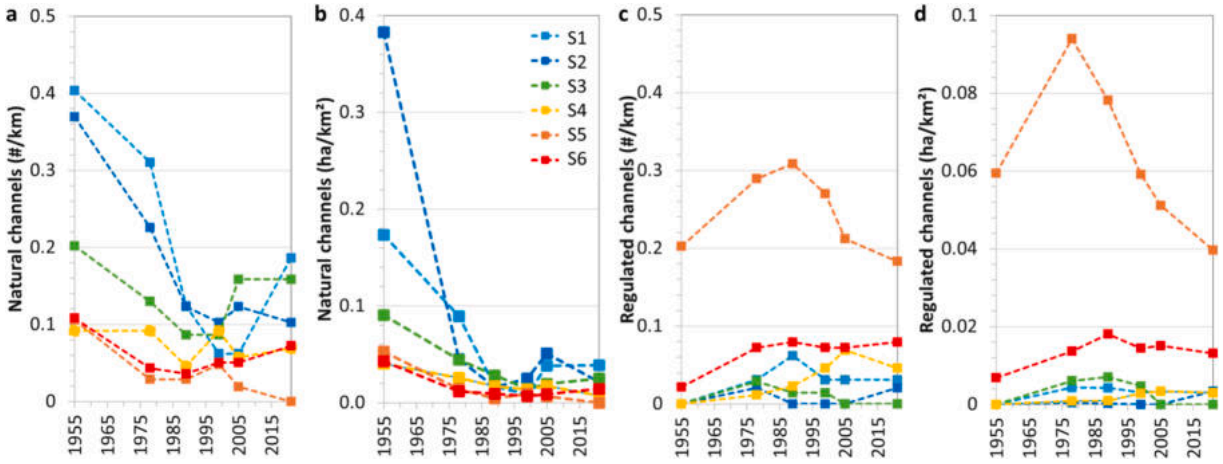

Fig. 6. Historical changes (1954–2021) along the six study segments of the Po River mainstem in terms of: (a) the number of natural secondary channels per unit segment length (#/km); (b) the combined area of natural secondary channels per unit segment active channel area (ha/km^2); (c) the number of regulated secondary channels per unit segment length (#/km); and (d) the combined area of regulated secondary channels per unit segment active channel area (ha/km^2).

and regulated) secondary channels hold information on in-channel sediment storage – on the evolving (im)balance between sediment supply and transport capacity (Schumm, 1977; Church, 2006). In this section, we present five case studies, characterized by varying degree of confinement, drawn from segments S2 to S6.

Proceeding in the downstream direction, the first case study in gravel-bed segment S2 (Fig. 7) represents a channel stretch initially characterized by transitional (or wandering) morphological pattern, high sinuosity, and largely natural margins (i.e., artificial confinement in 1954 is 22 %), with an additional 4 % of confinement imparted by natural hillslopes (see green linework in Fig. 7a–f). Across the 1970 s and 80 s sinuosity decreases because of point bar revegetation (see photo year 1975 in Fig. 7b) and subsequent meander abandonment (see photo year 1988 in Fig. 7c). Later, channel pattern configuration remains about the same until 2021 (Fig. 7d–f) at substantially constant anthropogenic confinement. In terms of active channel width, major narrowing between 1975 and 1988 (from 519 m to 314 m) is followed by a symmetrical rebound achieved in photo year 2021 (i.e., ACW = 518 m) (Fig. 7h). A similar historical trend, as also testified by the widespread occurrence of dynamic (vegetated and unvegetated) bars, suggests that alluvial sediment supply has not been a limiting factor across the entire study period, despite the increase in artificial confinement (from 39 % in 1979 to 64 % in 2021). This interpretation is further supported by the evolution of reference cross section A-A' (Fig. 7g and h), where on average, the foregoing trend of planimetric adjustment corresponds to substantial vertical equilibrium i.e., the bed aggrades cumulatively by 0.6 m between 1979 and 2005 and degrades by 0.8 m in 2021 (Fig. 7h).

The second case exemplifies the evolution of a channel stretch in gravel-bed segment S3, which in 1954 is characterized by a single-thread meandering pattern and largely natural margins (i.e., anthropogenic confinement equals 24 % in Fig. 8a). Between 1954 and 1975 channel sinuosity decreases substantially (Fig. 8b), and then retains about the same planimetric configuration until 1999 (Fig. 8c and 8d) at virtually unchanged confinement conditions. By 2005, we observe the growth of large alternating bars, which induce flow diversion and bank erosion on the opposite banks, leading to active channel widening (Fig. 8e). This tendency, which suggests a local increase in sediment supply (with respect to local transport capacity), continues until 2021, when, through the development of meanders, secondary channels and cutoffs, planform channel typology becomes transitional (or wandering) and major widening occurs (i.e., from 430 m in 2005 to 705 m in 2021; Fig. 8f). On average, this planimetric trend of adjustment is paralleled at reference cross section B-B' by more than 2 m of incision between 1969 and 1991, followed by sub-metric fluctuations until 2005 (Fig. 8g and h). Available cross-sectional data – note missing topography in 1955 – suggest that at this dynamic location correlation between planimetric and vertical channel changes is complex, beyond a straightforward narrowing-incision (or widening-aggradation) correspondence (Fig. 8h).

The third case study in sand-bed segment S4 differs from the former two in that, although characterized by comparable conditions of low anthropogenic confinement (i.e., 21 %), is far less dynamic (Suppl. Fig. 5). Indeed, at this site the channel pattern retains across the entire study period a simple, single-thread configuration, the main change being the obliteration of a vegetated island that imparts local narrowing following the installation of bank protections between 1954 and 1975. Interestingly, limited stretch-scale widening (i.e., from 425 m in 1954 to 499 m in 2021) is matched by concurrent average cross-sectional incision i.e., about 2.5 m at reference cross section C-C' (Suppl. Fig. 5h) and limited thalweg mobility after 1979 (Suppl. Fig. 5g). These observations, despite low anthropogenic confinement that should allow for lateral migration, point to sediment supply-limited conditions, as also supported by the limited extent of (vegetated and unvegetated) bars (Suppl. Fig. 5a–f).

The fourth example, located 30 km downstream of Isola Serafini Dam within sand-bed segment S5, represents a striking case of multi-thread, channel pattern transformation under conditions of increasing anthropogenic confinement (from 38 % to 50 % in Fig. 9a–f). Indeed, the entire hosting segment underwent major anthropogenic conditioning associated with the construction of the Isola Serafini Dam at the segment head (completed in 1958), and the massive emplacement of groins for ensuring navigation – part of the "*Sistemazione a corrente libera del Po*" project, which lasted from the 1930 s to the early 1960 s (Galvani and Pellegrini, 2009) (see Section 2 and the historical trend of the artificial margins in segment S5 i.e., orange linework in Fig. 4c). Accordingly, at this site characterized in 1954 by a transitional, multi-thread channel pattern, two major groins and widespread protection structures on the right bank stand out (Fig. 9a). Over time, as intense deposition is promoted behind the groins and the extent of lateral protection structures increases – thus preventing lateral migration and sediment recruitment from the banks – channel pattern evolves into a much narrower, single-thread meandering configuration (Fig. 9b and c). From 1988 onward, the planimetric configuration remains essentially on check, with further, less intense narrowing still occurring until 2005, as testified by the incorporation of the vegetated island into the adjacent alluvial plain (Fig. 9d and g). Strikingly, as the active channel narrowed by more than 500 m (i.e., from 813 m in 1954 to 318 m in 2021) (Fig. 9h), the riverbed average elevation dropped by 5.1 m (between 1954 and 2021) at reference cross section D-D' (Fig. 9g and h), pointing to persistent

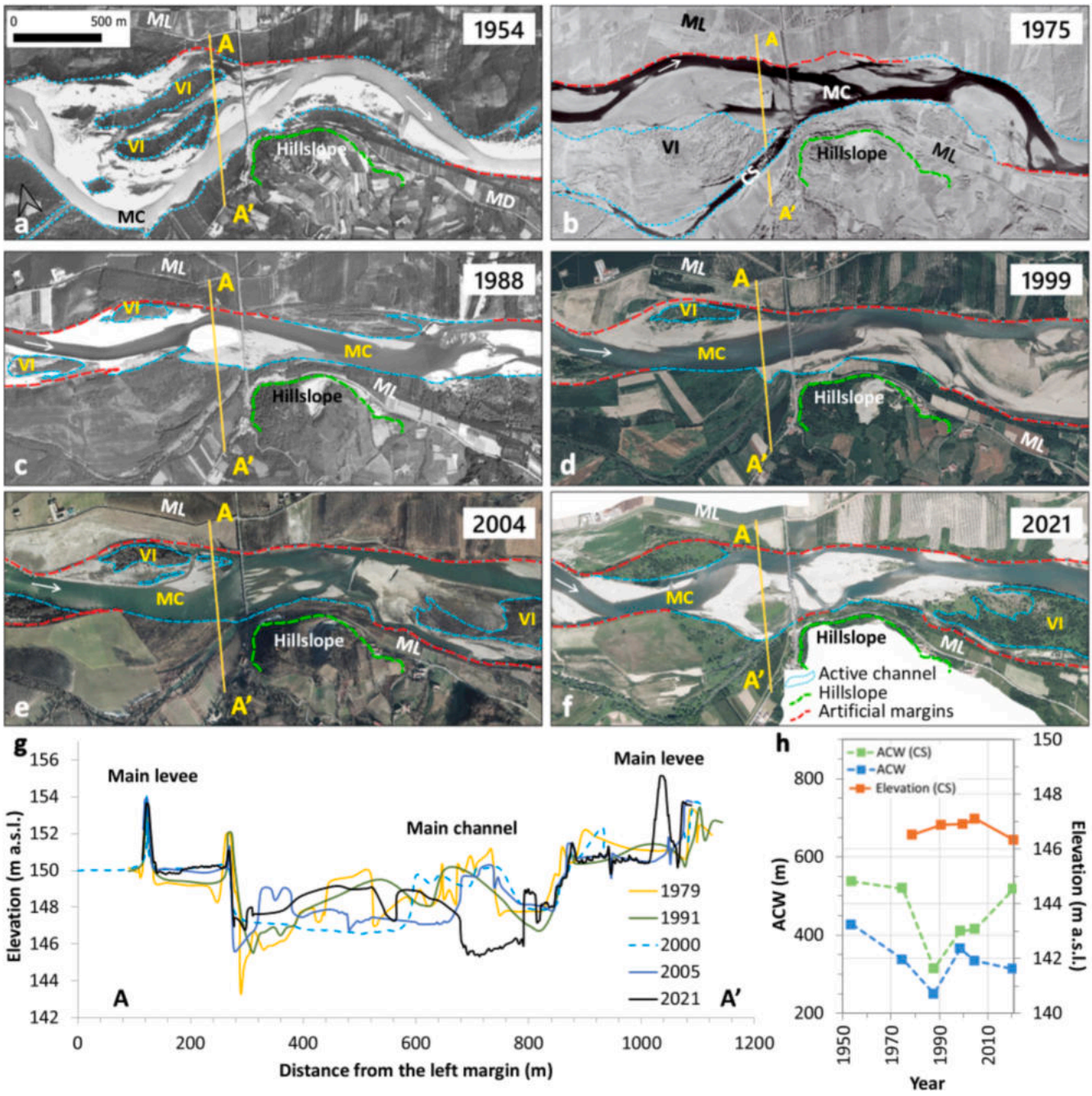

Fig. 7. Sample channel stretch, characterized by high anthropogenic confinement (i.e., 70 %, 2004), located at km 36 within segment S2, near the town of Crescentino (Vercelli). Planimetric evolution of the active channel across photographic years: (a) 1954; (b) 1975; (c) 1988; (d) 1999; (e) 2004; and (f) 2021. (g) Cross-sectional channel changes measured at A-A' in 1979, 1991, 2000, 2005 and 2021. (h) Historical trend in mean active channel bed elevation (red linework) and width (ACW) at the A-A' channel cross section (CS; green linework), and ACW across the entire river stretch (blue linework). In panels a through f, the white arrow denotes flow direction, and the yellow line marks the footprint of reference channel cross section A-A'. VI = vegetated island; MC = main channel; ML = main levee.

sediment starvation conditions through time. Overall, this local example reflects the segment-wide trend of historical adjustment characterized by sustained historical narrowing from 1954 until 2005 (cf., blue linework in Fig. 9h and Fig. 5e).

The last case study, located within segment S6, illustrates the effects of consistent high confinement conditions (i.e., 73 %). At this site, in which the active channel is bound by levees that were built in the 1930 s, apart from the varying level of submergence in the six photographic years, we observe no planimetric channel adjustment between 1954 and 2021 (Fig. 10a–f). In this context, substantial stability in ACW (Fig. 10h) is matched at reference cross section E-E' by vertical stability, after thalweg migration occurred between 1954 and 1978 (Fig. 10g). When averaging bed-level cross-sectional changes, a maximum incision of slightly over 1 m is observed (Fig. 10h). Overall, owing to the high levels of submergence and planform stability since 1978, this highly confined stretch resembles closely the morpho-dynamics of a graded canal.

4.5. Geomorphic changes downstream of the Isola Serafini complex

To investigate the anomalous narrowing trend of segment S5 further (Fig. 5e), also in light of the drastic bed incision observed locally (Fig. 9), we illustrate the historical evolution (1889–2005) of this river portion

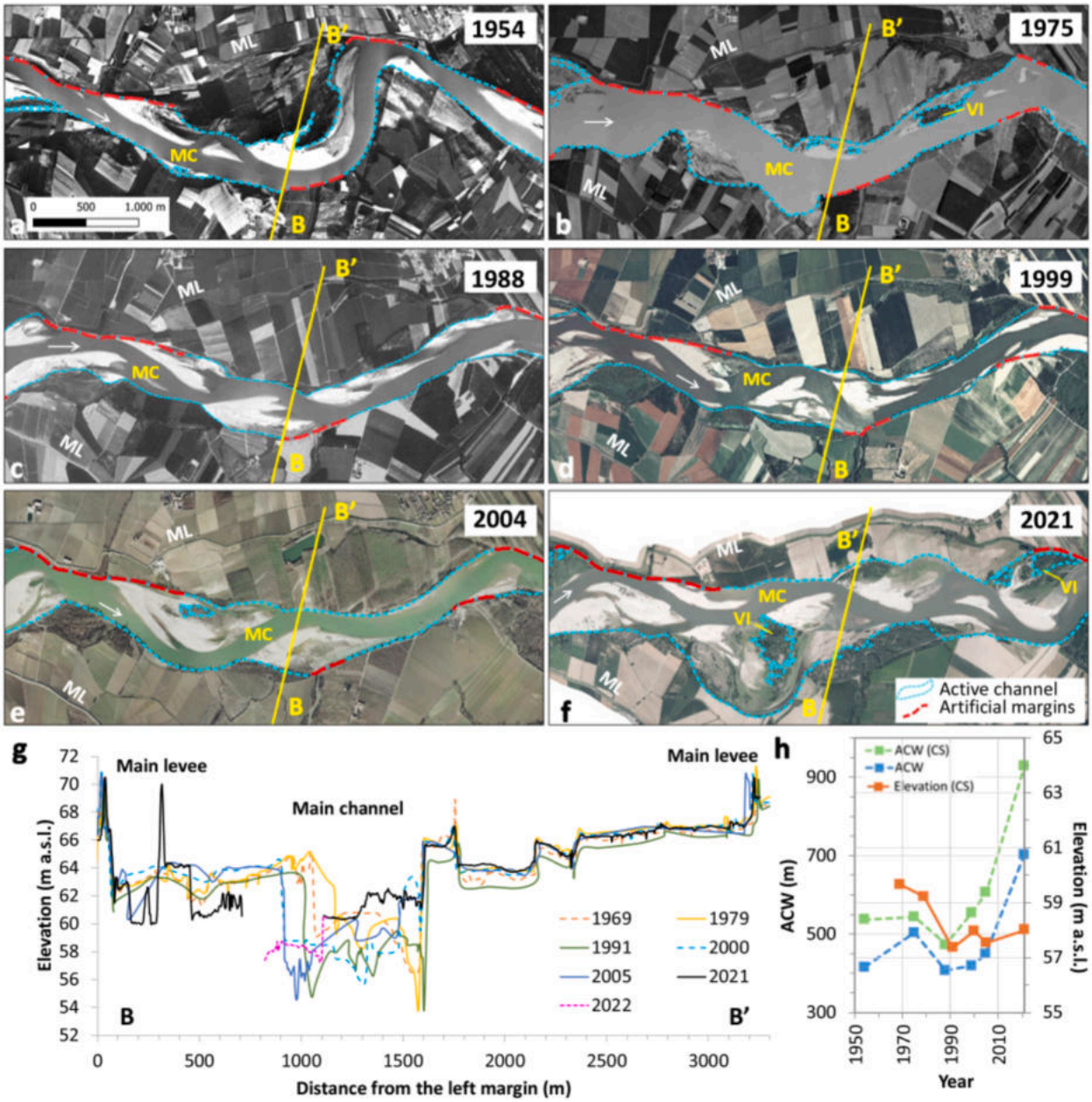

Fig. 8. Sample channel stretch, characterized by low anthropogenic confinement (i.e., 24 % in 2004), located at km 130 within segment S3, near the town of Voghera. Planimetric evolution of the active channel across photographic years: (a) 1954; (b) 1975; (c) 1988; (d) 1999; (e) 2004; and (f) 2021. (g) Cross-sectional channel changes measured at B-B' in 1969, 1979, 1991, 2000, 2005 and 2021–2022. (h) Historical trend in mean active channel bed elevation (red linework) and width (ACW) at the B-B' channel cross section (CS; green linework), and ACW across the entire river stretch (blue linework). In panels a through f, the white arrow denotes flow direction, and the yellow line marks the footprint of reference channel cross section B-B'. VI = vegetated island; MC = main channel; ML = main levee. Note high flow conditions in 1975.

before and after the construction of the Isola Serafini complex (i.e., the hydropower dam and the adjoining navigation bypass). Subsequently, to ascertain the extent to which the reduced rates of planimetric narrowing in 2005–2021 may underlie a possible regain of (nearly) equilibrium dynamics, we exploit two sets of repeat high-resolution (bathymetric and subaerial) topographic surveys (Table 2), and constrain the 2005–2021 sediment budget via thresholded DoD (DEM of Difference) analysis (Wheaton et al., 2010) (Fig. 11a).

The dam, which was built following the 1951 meander cutoff at Isola Mezzadra (Fig. 11b), on one hand prevented headward bed incision upstream of the cutoff – a response that typically follows such an abrupt morphological change due to the higher slope and lesser sinuosity of the newly formed channel; on the other hand, it halted downstream sediment continuity. The combined effects of the dam and the navigation bypass – a highly confined canal dug along the southern branch of the paleo meander (see Fig. 11b and Suppl. Fig. 6) – resulted in metric decadal (1954–2005) rates of incision between the dam and the confluence with the Taro River, as shown by the control section near Cremona (Suppl. Fig. 6c; AdBPo, 2008a) and by the sample channel stretch located 18 km further downstream (Figs. 9 and 11). These incision rates are consistent with the concurrent active channel narrowing (Fig. 5e), and therefore support that in 1954–2005 segment S5 underwent major degradation dynamics.

In this context, the 2005–2021 DoD analysis clarifies that the sudden concurrent decline in planimetric narrowing at S5 (Fig. 5e) reflects weakly degrading dynamics approaching at the segment scale a quasi-

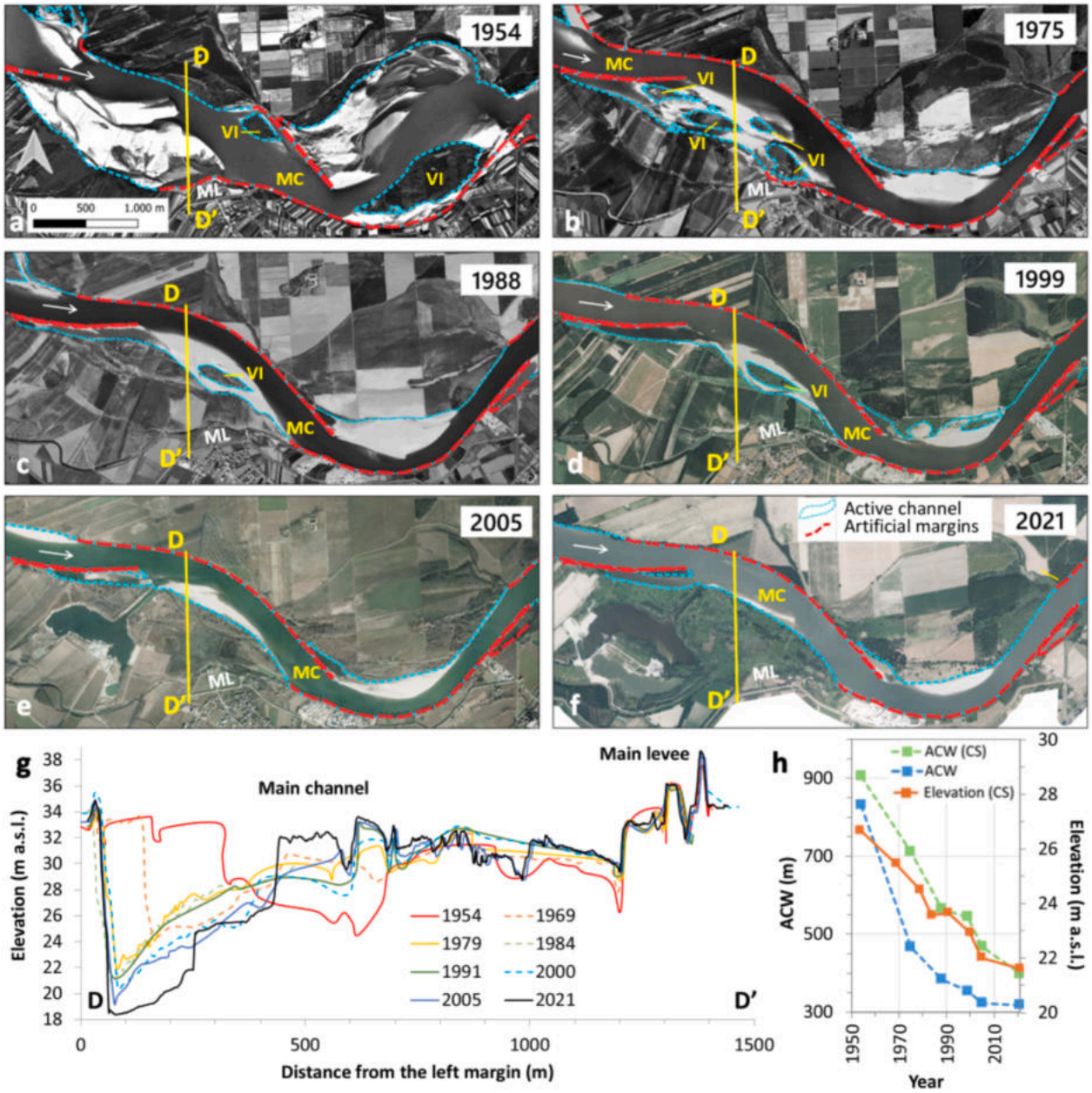

Fig. 9. Sample channel stretch, characterized by a degree of anthropogenic confinement that increases from 38 % (1955) to 50 % (2021), located 18 km downstream of the Isola Serafini navigation bypass in segment S5. Planimetric evolution of the active channel across photographic years: (a) 1954; (b) 1975; (c) 1988; (d) 1999; (e) 2004; and (f) 2021. (g) Cross-sectional channel changes measured at D-D' in 1954, 1969, 1979, 1984, 1991, 2000, 2005 and 2021. (h) Historical trend in mean active channel bed elevation (red linework) and width (ACW) at the D-D' channel cross section (CS; green linework), and ACW across the entire river stretch (blue linework). In panels a through f, the white arrow denotes flow direction, and the yellow line marks the footprint of reference channel cross section D-D'. VI = vegetated island; MC = main channel; ML = main levee.

equilibrium state (Fig. 11c). Specifically, it depicts systematic reach-scale departures from sedimentary balance, with volumetric net change shifting progressively from degradation to aggradation as one moves away from the navigation bypass (Table 5 and Fig. 11c).

5. Discussion

5.1. Historical narrowing of large rivers and quantitative information on confinement

Over the last two centuries, much alike for the Po River mainstem, large rivers across France and Spain have experienced major channel planform and bed-level changes following extensive human interventions. Interestingly, as will become clear, none of these fluvial systems appeared to display a post-disturbance phase of recovery in the 1990 s and later, in contrast with the historical adjustment documented in the Po River's main tributaries (Fig. 1a) and in the more confined segments S4, S5, and S6 (Fig. 5).

Accordingly, in the Garonne River, anthropogenic pressures of some intensity commenced in the 19th century in the upstream and middle portions and progressively extended downstream after the 1940 s. David et al. (2016) document that the cumulative length of protected banks in the Mid Garonne River increased from none in 1955 to over 30 km in 1985 and remained substantially unchanged until at least 2010. Levees in the urban sectors of Toulouse rose in length from ~ 4 km in 1950 to 12 km in 1970 and up to 15 km by 2010. In addition, gravel mining,

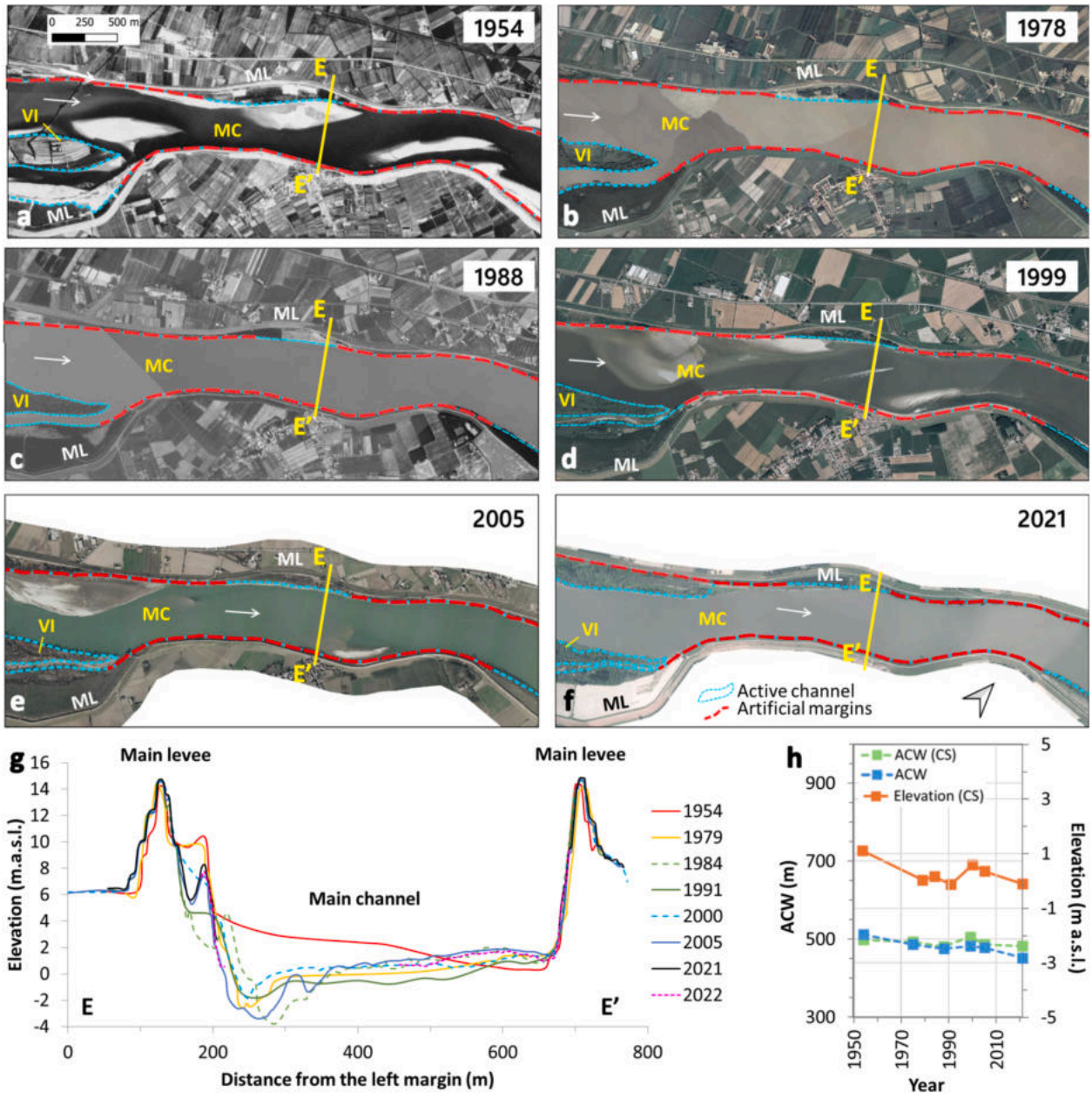

Fig. 10. Sample channel stretch, characterized by high anthropogenic confinement (73 %), located at km 443 within segment S6, near the town of Ferrara. Planimetric evolution of the active channel across photographic years: (a) 1954; (b) 1975; (c) 1988; (d) 1999; (e) 2004; and (f) 2021. (g) Cross-sectional channel changes measured at E-E' in 1954, 1979, 1984, 1991, 2000, 2005 and 2021–2022. (h) Historical trend in mean active channel bed elevation (red linework) and width (ACW) at the E-E' channel cross section (CS; green linework), and ACW across the entire river stretch (blue linework). In panels a through f, the white arrow denotes flow direction, and the yellow line marks the footprint of reference channel cross section E-E'. VI = vegetated island; MC = main channel; ML = main levee.

particularly between the 1960 s and 1990 s, is considered to have further impacted this river portion, which overall narrowed by ~ 40 % between 1868 and the early 2000 s without showing any hint of planimetric rebound.

Differently from what observed in large tributaries of the Po River (Fig. 1a), the Middle Loire River experienced consistent narrowing in 1955–1984 (i.e., 0.5 m/yr), a trend that was found to persist and that accelerated up to 1.7 m/yr in 2002–2010 (Latapie et al., 2014). This style of adjustment was interpreted to reflect the cumulative impacts of channel embankments (13th–18th centuries), groins (19th century), hydroelectric dams and large-scale mining operations from the 1950 s to the early 1990 s. Concurrently to narrowing, a high degree of confinement – although this could not be constrained quantitatively – is thought to have imparted planform stability, while the mainstem continued to incise, vegetated islands degraded, and secondary channel underwent generalized disconnection. These latter dynamics of channel pattern simplification resemble what documented in sections 4.3 and 4.4 along the Po River.

In the Lower Rhône, comparable interventions – construction of defense works and groins (1870–1920 s), dams (1950 s–1970 s), and intensive sediment mining (1970 s–1990 s) – transformed the channel pattern from braided to a sinuous, single-thread one. Between 1860 and 2006 channel narrowing ranged from 25 % to ~ 45 % – percentages that are in line with those documented in the Po River's highly confined segments S4, S5 and S6 (Fig. 5 and Suppl. Fig. 7) – with no glimpse of planimetric re-widening observed (Provansal et al., 2014).

In Spain, the Ebro River underwent rapid artificialization associated with the installation of defense works between the 1960 s and 1980 s.

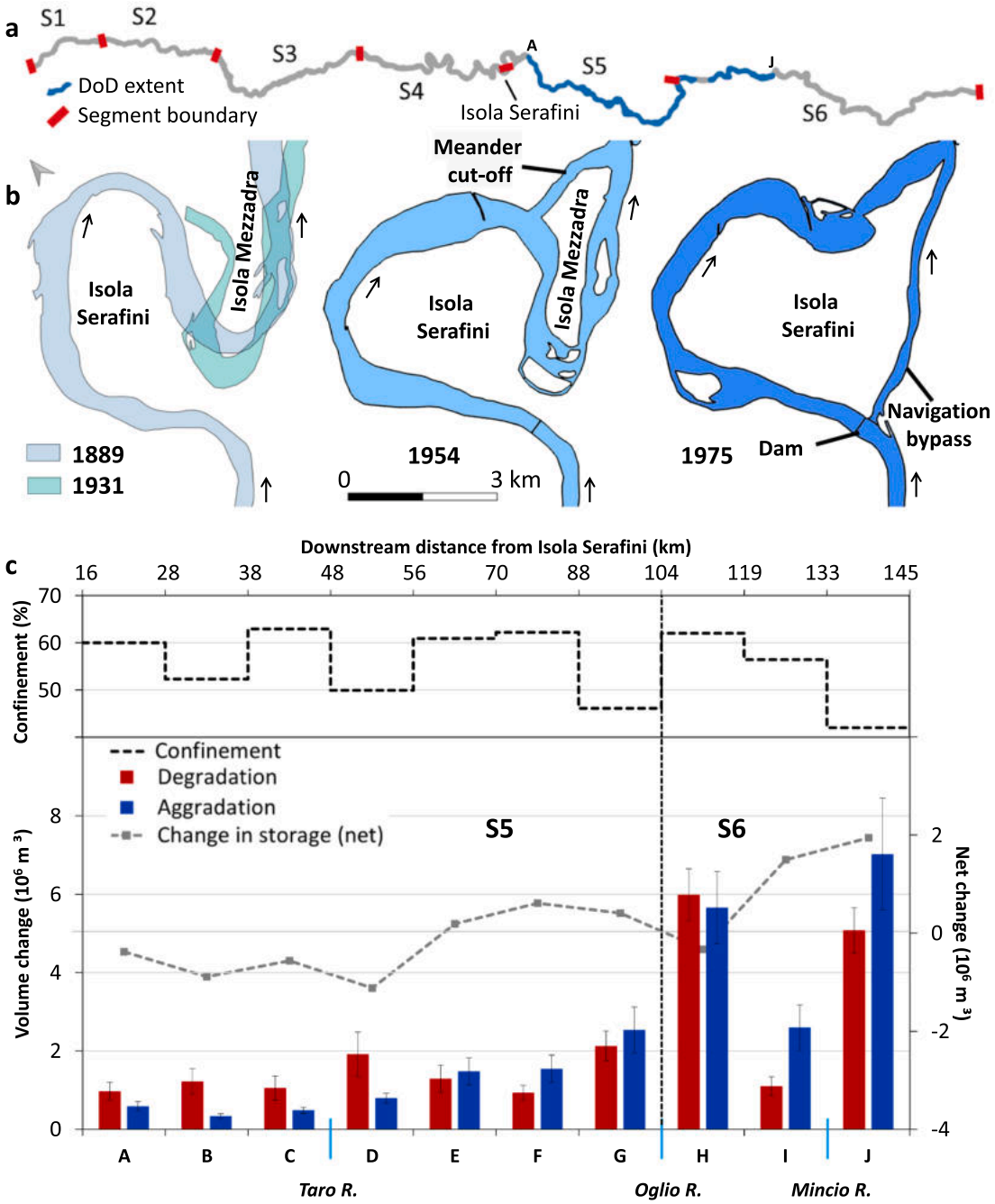

Fig. 11. Plan view of the: (a) 2005–2021 DoD extent (blue area) within the study mainstem (grey area); and (b) historical evolution of the Isola Serafini area before and after the construction of the hydroelectric dam and the navigation bypass (the historical mapping in 1889 and 1931 are provided by AdBPo). (c) Volume change associated with bed degradation (red bars), aggradation (blue bars), and the resulting (net) change in alluvial storage (dashed gray line) across 88 km in segment S5 and 36 km in segment S6. Intra-segment subdivisions correspond to the morphologically homogeneous reaches proposed by Brenna et al. (2024). Note that the DoD starts at reach A, downstream of the junction with the navigation bypass, and ends at reach J, about 10 km downstream of the Secchia River confluence. In reach H, a 5-km bathymetric data gap exists. In panel a, the dashed black line indicates anthropogenic confinement at the reach scale in year 2005. For a photographic plan view of the historical evolution (1954–2021) around Isola Serafini please see Suppl. Fig. 6 Error bars refer to values below the minLoD (minimum level of detection), calculated through the propagation of the DTM errors using a 95 % confidence interval.

Specifically, the linear extent of levees rose from ~ 75 km in 1955 to over 375 km in 1985, and that of other lateral defenses peaked from ~ 25 km to ~ 125 km (Ollero, 2010). These structures are regarded responsible for the drastic reduction in sinuosity and active channel width, which ultimately led to near-complete stabilization by the mid-1980 s (Ollero, 2010; Magdaleno et al., 2012). Overall, two studies concur that the Ebro River narrowed by 50-to-60 % (1927–2007) (Ollero, 2010) and ~ 50 % (1927–2003) (Magdaleno et al., 2012). Similar percentages of width shrinkage are comparable with that reported for tightly confined segment S5, downstream of Isola Serafini Dam (Fig. 5e and Suppl. Fig. 7e). Finally, in the Upper Cinca River, a Pyrenean tributary of the Ebro River, Llena et al. (2020) reports a lower combined historical narrowing (i.e., ~33 % in 1927–2015), with the most pronounced shrinkage (i.e., 15 %) recorded between 1984 and 1997. Also in this case, narrowing was interpreted as the result of post-1920 s afforestation, combined with extensive gravel mining conducted

Table 5
2005–2021 volume change associated with bed aggradation, degradation, and the resulting net change (i.e., change in alluvial sediment storage) across 10 homogeneous channel reaches within segments S5 and S6, downstream of the Isola Serafini navigation bypass.

Reach	Anthropogenic confinement (%)	Volume change (10^6 m^3) Degradation	Aggradation	Net change
A	63.6	0.97 ± 0.23	0.59 ± 0.11	−0.38 ± 0.25
B	55.6	1.23 ± 0.33	0.34 ± 0.06	−0.89 ± 0.33
C	64.6	1.05 ± 0.31	0.49 ± 0.08	−0.56 ± 0.32
D	43.0	1.92 ± 0.57	0.79 ± 0.13	−1.12 ± 0.58
E	60.0	1.29 ± 0.35	1.48 ± 0.35	0.19 ± 0.49
F	59.2	0.94 ± 0.19	1.55 ± 0.35	0.61 ± 0.40
G	61.2	2.13 ± 0.38	2.53 ± 0.59	0.40 ± 0.70
H	68.6	5.99 ± 0.67	5.66 ± 0.92	- 0.33 ± 1.14
I	65.0	1.10 ± 0.24	2.60 ± 0.58	1.50 ± 0.63
J	48.8	5.08 ± 0.57	7.02 ± 1.43	1.94 ± 1.54

in the mid-1970 s and embankments installed in the mid-1980 s.

While the behavior of the foregoing case studies shares consistent historical narrowing, the role played by bank protections and levees over time – and therefore the likely reason for the lack of partial recovery to larger channel widths – is difficult to guess. This is because in two instances only the temporal evolution of bank protections and levees (i.e., rigid artificial margins) could be documented, and in none of them the evolving percentage of anthropogenic confinement was quantified.

5.2. *Confining threshold to planimetric adjustment*

Quantitative information on confinement across decades improves our ability to infer possible controls exerted by this type of anthropogenic forcing on the relevant geomorphic response of large rivers. Based on the historical trend of planimetric adjustment, the Po River may be broadly subdivided into two halves: a proximal one encompassing the dominantly gravel-bed segments S1, S2 and S3, and a distal counterpart encompassing the sand-to-finer bed segments S4, S5 and S6. The former set, characterized by initial anthropogenic confinement < 28 % (i.e., between 18 % and 27 %) (Fig. 11b), shares a trend of generalized channel narrowing (1955–1989), followed by partial recovery to wider, transitional channel patterns (1989–2021), as shown at sample channel stretches within segments S2 (Fig. 7) and S3 (Fig. 8). This behavior broadly agrees with prior findings and conceptualizations about the recent adjustment of selected unconfined reaches from European rivers (e.g., Liébault and Piégay, 2001, 2002; Surian and Rinaldi, 2003; Surian et al., 2009; Comiti, 2012; Bollati et al., 2014; Scorpio et al., 2024), and the Po River tributaries in particular (Fig. 1a). By contrast, the latter set of segments, where initial anthropogenic confinement is higher (i.e., between 37 % and 46 %), displays continuous historical narrowing, adjacent segments S6 and S5 stand out respectively for the least (6 %, or 26 m) and the largest (53 %, or 367 m) median width reduction since 1954 (Fig. 6 and Suppl. Fig. 7). This second style of adjustment mimics the one just described across large rivers in France and Spain, which share comparable multidecadal ranges of percent active channel narrowing (e.g., Ollero, 2010; Magdaleno et al., 2012; Latapie et al., 2014; Provansal et al., 2014; David et al., 2016).

With respect to the possible causal linkages between channel narrowing and in-channel mining, the one-order of magnitude reduction of in-channel mining concessions – legally imposed since the early 1980 s (i.e., since 1982 within rivers of the Emilia-Romagna region) – appears to have fostered a significant rebound in active channel width along the three proximal mildly confined segments. This rebound, which is indicative of increased in-channel sediment availability, reflects a similar trend documented further upstream along unconfined reaches of the adjoining main tributaries i.e., Stura di Lanzo, Orco and Scrivia (Pellegrini et al., 2008; Surian et al., 2009; Mandarino et al., 2019) (Fig. 1a). In contrast, the three distal, strongly confined segments have remained insensitive, as they continued narrowing between 1978 and 1989 at unchanged rates (Fig. 11c), despite the post-1990 s rewidening observed further upstream in segments S1, S2 and S3, and along unconfined reaches of the adjoining tributaries i.e., Trebbia, Taro and Panaro (Rinaldi et al., 2008; 2010; Bollati et al., 2014; Clerici et al., 2015) (Fig. 1a). In other words, the planimetric signal of adjustment observed along the main tributaries and in the proximal gravel-bed segments did not propagate down to S4, S5 and S6.

Besides the possible contribution to resistance of higher bank cohesion in segments S5 and S6 (given the higher amount of finer fractions) (Table 4 and Fig. 4a), we propose that this dichotomic behavior between the proximal and the distal segments has to do chiefly with the contrasting degrees of anthropogenic confinement when mining activity was at its historical peak and about to collapse (i.e., photographic years 1975–78): respectively < 33 % in S1-S3 and > 45 % in S4-S6 (Fig. 12b). Following this logic, the relative increase in alluvial sediment supply associated with in-channel mining collapse, both in the Po mainstem and along its main tributaries (Fig. 2b), would not have imparted a detectable change to the ACW trajectory in S4, S5 and S6 because of their reduced potential for lateral migration against dominantly fixed and rigid artificial channel margins. Apparently, a similar barrier to change (sensu Brunsden, 1993) was able to hold independently of hydrometeorological forcing, since the two clusters of large historical floods occurred in 1976–79 and 1994–2002 (Fig. 2a) likely fostered the rebound in S1, S2 and S3, but did not alter the long-term narrowing trend in S4, S5 and S6. At least in planimetric terms, an anthropogenic confinement approaching or > 45 % may be viewed as an effective threshold beyond which the study segments have become insensitive to geomorphic perturbations travelling down the fluvial system (Brunsden and Thornes, 1979; Schumm, 1985).

This confining threshold appears to apply to natural secondary channel area (per unit segment active channel area), as the relevant trends of the proximal (less confined) segments S1, S2 and S3 are well discriminated from the distal (more confined) counterparts, which display distinctively lower values and do not show significant rebounds in the 1990 s (Fig. 12d). As a possible complement to active channel width, this variable, which could be extracted (semi)automatically by means of CNN-based classification approaches (e.g., Carbonneau et al., 2020; Wieland et al., 2023), appears to be suitable for tracking changes in channel pattern, and therefore, indirectly, for the rapid evaluation of alluvial sediment storage depletion and recovery through time.

The resisting effect of anthropogenic confinement against lateral migration potential – that is, the ability to accommodate increased sediment supply through active channel widening – may be inferred from comparing gravel-bed segments S1 and S2. Accordingly, the consistently higher degree of historical confinement in S2 (Fig. 12b), compared to S1, would explain: (i) S2′s smaller decadal fluctuations in median ACW; and (ii) very similar (and sometimes even smaller) median ACW values (Fig. 12c), and interquartile ACW percent changes since 1955 (Suppl. Fig. 7a and 7b), despite S2 greater contributing area (Table 4), and therefore against principles of downstream hydraulic geometry along channels with comparable bed texture (Table 4 and Fig. 4a) (Leopold and Maddock, 1953; Ferguson, 1986). It should be noted that, in part, the reduced and more stable median ACW values in S2, may have to do with the Lanza Dam (built in 1874) (Fig. 12a).

Among the highly confined sand-to-finer bed segments, comparison of the historical trend in median ACW between S4 and S6 suggests that

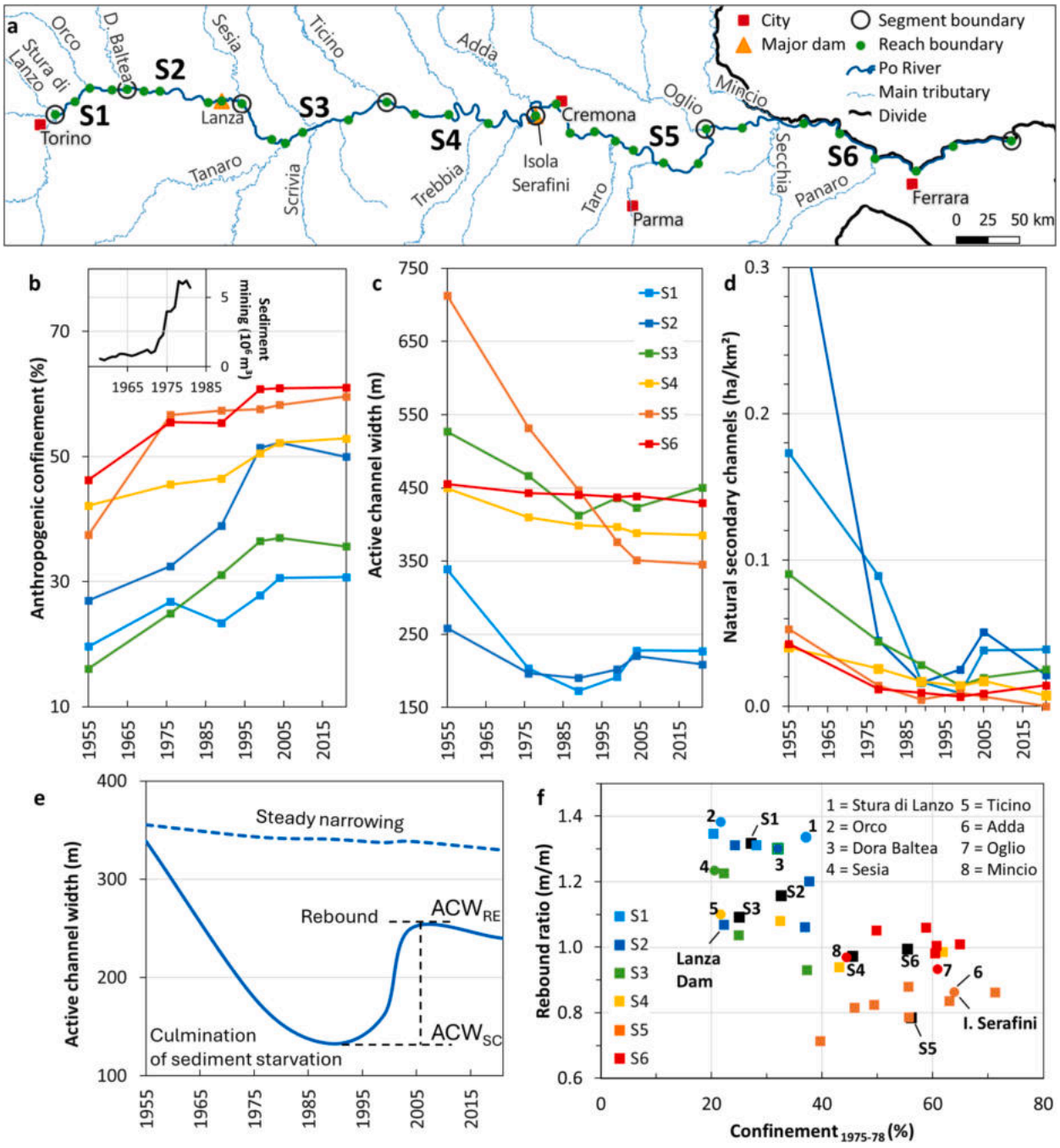

Fig. 12. (a) Map of the Po River mainstem subdivided into six segments and thirty-three reaches, showing the location of the main tributaries and the main dams between the confluence with Stura di Lanzo River and the Po delta apex. Reaches 20-29 correspond to those labelled as A-J in Table 5 and Fig. 11c. Historical trend (1954–2021) of the six study segments with respect to: (b) the degree of anthropogenic confinement; (c) the median active channel width calculated over 500-m channel stretches; and (d) the combined area of natural secondary channels per unit active channel footprint. (e) Schematic view of the rebound ratio (RR) – the ratio between active channel width at the peak of planimetric recovery to wider channel configuration (ACW_{RE}) and the minimum reached at the culmination of sediment starved conditions (ACW_{SC}); and (f) Rebound ratio (RR) as a function of anthropogenic confinement in 1975–78 (i.e., when in-channel mining was at its historical peak and about to collapse) across the study segments (black symbols) and reaches (color-coded symbols denote different hosting segments). Circles designate reaches hosting confluences with the main tributaries (i.e., labeled 1 through 8) at the relevant upper ends.

higher confinement in the latter segment – from 42 % (1955) to 53 % (2021) in S4, and from 46 % (1955) to 61 % (2021) in S6 – would ensure higher planimetric stability (Suppl. Fig. 7), much alike the intended functioning of an artificial canal (Fig. 12c). This situation is well exemplified by the local case study in S6 (Fig. 10), where the main levees commonly coincide with the margins of the active channel bed. Alone, high confinement would not justify the anomalous behavior of segment S5, which, despite sharing a similar history of anthropogenic confinement (i.e., confinement rises by about 20 % in 1954–2005; Fig. 12b), has evolved very differently from contiguous S4 and S6. In principle, the intense narrowing between 1954 and 2005 may be ascribed to the installation of navigation groins, whose density is much higher in S5 (439 m/km), compared to S6 (129 m/km), and S4 (21 m/km) (Table 4). This explanation, however, would hold for the 1950 s-1970 s period only – as shown by Brenna et al. (2024) and here exemplified in the relevant case study (Fig. 9).

As previously shown in the DoD analysis, the 2005–21 sediment budget suggests that the highly confined segment S5 has attained weakly degrading sediment dynamics only after 2005 – following at least 50 years of intense narrowing (Fig. 12c) and bed degradation (Fig. 9h and Suppl. Fig. 6c) – and that this imbalance has been dictated in 1954–1988 by in-channel mining in conjunction with the installation of navigation groins (i.e., Fig. 9a–f), and later by the Isola Serafini complex. The latter, by drastically reducing sediment supply/transfer to segment S5, has likely delayed the local pace of adjustment to a new quasi-equilibrium state by at least 40 years. The assessment of such time scales of adjustment complements existing knowledge on the upstream effects of the dam (i.e., Maselli et al., 2018), and enriches prior accounts according to which the Po River would have regained substantial balance since the mid-1980 s following a reduction in anthropogenic pressures (e.g., Castiglioni et al., 1999; Marchetti, 2002).

Ongoing bed degradation across the 40-km stretch downstream of the Isola Serafini bypass, suggests considering more sustainable operational alternatives for this regulated complex, as well as a series of nature-based solutions for recovering sedimentary balance. The latter measures will involve re-activation of the main sources of sediment supply, including the re-opening of regulated secondary channels, and a reconfiguration of some bank protections to warrant greater room for alluvial storage and channel migration.

5.3. *From segments to reaches: Threshold consolidation and insights*

Grouping the 500-m channel stretches into thirty-three morphologically homogeneous reaches (see Section 3) offers the opportunity to shed light on the intra-segment variability that characterizes planimetric adjustment. In particular, we wish to explore the extent to which an increase in spatial resolution (i.e., from six segments to thirty-three reaches) would allow to better constrain the confinement threshold for planimetric adjustment provisionally identified in section 4.3 and discussed above. To this end, we represent the so-called "rebound ratio" (RR) – the ratio between active channel width at the peak of planimetric recovery to wider channel configuration (ACW_{RE}) and the minimum reached at the culmination of sediment starved conditions (ACW_{SC}) (see definition in section 3.3; Fig. 12e) – as a function of anthropogenic confinement in 1975–78 (Fig. 12f), when mining was at its historical high and about to collapse. Accordingly, RR $>$ 1.1 marks a regain in active channel width $>$ 10 %, and RR $<$ 1 indicates no rebound to larger channel configuration, but a tendency to planimetric narrowing.

This reach-based representation, while broadly confirming the segment-based findings, allows refining previous generalizations while gaining further insights. Specifically, an abrupt barrier to channel-reach rewidening is apparent for confinement $\geq$ 40 %, which is about 5 % lower than how previously hinted at the segment scale. Beyond this threshold, only three reaches in S6 (out of seventeen) exhibit modest rewidening (i.e., RR $<$ 1.1), while the rest shows no rebound and continues to narrow. Conversely, for confinement $<$ 40 %, a rebound in active channel width is observed in all sixteen cases (i.e., up to RR = 1.38) but one in S3, where narrowing continues.

Spearman's rank correlation analysis conducted at the reach scale corroborates the inverse RR-confinement relation previously suggested across segments, which now becomes statistically significant at the 0.001 level (n = 33; coefficient = − 0.72; p-value $<$ 0.001).

Reach-based insights include: (i) the stabilizing effect of the Lanza Dam in R8, which displays an RR of just 1.07, despite a 22 % of confinement; (ii) the upstream stabilizing effect of the Isola Serafini Complex in R18 (Maselli et al., 2018), which shows no rebound (RR = 0.99), despite a confinement of 25 %; (iii) the rebound amplification in reaches fed by prominent Alpine tributaries, as exemplified by R3 (Orco River), R5 (Dora Baltea River), R10 (Sesia River), and R15 (Ticino River), respectively characterized by rebound ratios of 1.38, 1.30, 1.23, and 1.16, which represent peak values within the hosting segments, with the latter possibly buffered by Lake Maggiore; and (iv) the lack of confluence effects in highly confined and regulated reaches fed by tributaries originating from large Alpine lakes, as shown in R19 (Adda River), R27 (Oglio River), and R29 (Mincio River), where no rebound is observed (i.e., RR respectively equals 0.86, 0.98, and 0.93).

When opportunely validated and regionally parameterized – for example by means of sediment provenance analysis conducted at strategic tributary junctions (e.g., Garzanti et al., 2012, 2016) – the confining threshold here constrained could be used as a minimum reference target to pursue in river re-naturalization plans that aim to provide "strangled" rivers with more room for lateral mobility, while reducing flood risk, affording more flexibility to adapt to changing climate, and ultimately preserving (or regaining) relevant ecological services (Brierley et al., 2023).

6. Conclusions

In a historical context of increasing anthropogenic confinement, our results portray a more complex picture of adjustment than that described for largely unconfined reaches across European rivers (e.g., Liébault and Piégay, 2001; Surian and Rinaldi, 2003; Scorpio et al., 2024). By considering the entire Po River mainstem we extend previous results, quantify the relevant degree of anthropogenic confinement over time, and characterize fluvial adjustment in relation to varying conditions of confinement. Specifically, despite the relaxation of anthropogenic pressures occurred in the last four decades, we find that the current pace of planimetric and volumetric recovery to be still strongly conditioned by the spatial distribution of artificial confining structures, and more locally by the hydroelectric Isola Serafini complex.

Exploiting the order of magnitude rise and fall in mining activity (i.e., early 1970 s to early 1980 s), which we regard as the major decadal perturbation in alluvial sediment supply (or in-channel storage) – possibly amplified by the subsequent occurrence of the largest floods since 1950 – we tested the planimetric sensitivity of the Po River segments in relation to varying anthropogenic confinement. After four decades of narrowing, the historical adjustment of active channel width along the main Po River tributaries underwent a phase of partial rewidening from the early 1990 s onward. This phase of recovery to wider channel configurations is reflected downstream in the proximal segments S1-S3, characterized by contingent anthropogenic confinement $<$ 33 %. In contrast, a confinement threshold approaching 45 % was found to prevent planimetric recovery further downstream in segments S4-S6, where the narrowing trend persisted.

When partitioning segments into thirty-three (finer) reaches this confining threshold is refined to 40 %, and diverging adjustment styles become apparent (i.e., rebound vs. no rebound). In particular, representing the rebound ratio – a dimensionless metric of planimetric recovery since the historical low experienced in the 1980 s – as a function of contingent confinement supports that above threshold conditions: (i) dams can greatly depress or completely erase rebound potential; and (ii) major tributary confluences typically amplify the rebound, thus enhancing sensitivity to an increase in sediment supply.

Our work underlines the significance of anthropogenic confinement on the contemporary functioning of large rivers. For an improved definition of effective confining thresholds, further work is needed across a broader range of physiographic settings. To this end, we believe greater emphasis should be placed on anthropogenic confinement, which could complement current awareness on river (longitudinal and lateral) fragmentation (e.g., Grant et al., 2017; Mason et al., 2025) and barrier removal (e.g., Grant et al., 2012; Belletti et al., 2020) towards more efficient and sustainable management strategies.

CRediT authorship contribution statement

Michael Vinicius de Sordi: Writing – review & editing, Writing – original draft, Project administration, Methodology, Investigation, Formal analysis, Data curation. **Giovanni Vezzoli:** Writing – review &

editing, Methodology, Investigation, Formal analysis. **Francesco Brardinoni:** Writing – review & editing, Writing – original draft, Supervision, Methodology, Investigation, Funding acquisition, Formal analysis, Conceptualization.

Declaration of competing interest

The authors declare that they have no known competing financial interests or personal relationships that could have appeared to influence the work reported in this paper.

Acknowledgements

This work was jointly funded by the Autorità di Bacino Distrettuale del Fiume Po (AdBPo) through project R37/2022: "Aggiornamento del programma di gestione del Fiume Po e integrazione con i rami del delta" (CUP F22G16000000001) and the University of Bologna. We greatly acknowledge collaborative support granted by AdBPo personnel, and Tommaso Simonelli in particular, for sharing knowledge on the Po River and for granting access to existing documentation and to cartographic/photographic information. We thank Stefano Campus of Regione Piemonte (Direzione Ambiente, Energia e Territorio, Settore Sistema Informativo Territoriale e Ambientale) for granting access to 1954 and 1975 aerial photos of the Po River within the borders of Regione Piemonte. Stimulating discussions with Simone Bizzi, Michele Bolla Pittaluga, Andrea Brenna, Stefano Lanzoni and Nicola Surian helped broadening the paper perspective, as well as gaining insights on hydraulics, ongoing sediment dynamics and outstanding management issues. Constructive and thorough reviews by the AE Jantene Baartman and two anonymous reviewers helped improving the paper structure and presentation.

Appendix A. Supplementary data

Supplementary data to this article can be found online at https://doi.org/10.1016/j.catena.2025.108908.

Data availability

Data will be made available on reasonable request.

References

AdBPo., 2006. Autorità di Bacino Distrettuale del Fiume Po, 2006. Stralcio "intermedio", Programma generale di gestione dei sedimenti alluvionali dell'alveo del fiume Po – Stralcio confluenza Tanaro, confluenza Arda: deliberazione n. 20 del Comitato Istituzionale del 5 aprile 2006, Parma. 129 p. In Italian.

AdBPo., 2008a. Autorità di Bacino Distrettuale del Fiume Po. Il recupero morfologico ed ambientale del fiume Po: Il contributo del Programma generale di gestione dei sedimenti del fiume Po, 27 p. In Italian.

AdBPo., 2008b. Autorità di Bacino Distrettuale del Fiume Po. Atlante Geomorfologico del Fiume Po. Fiume Po da confluenza Stura di Lanzo a Pontelagoscuro. Parte 1: Cartografia delle variazioni planimetriche dell'alveo del fiume Po, 97 p. In Italian.

AdBPo., 2008c. Autorità di Bacino Distrettuale del Fiume Po, Stralcio "di valle", Programma generale di gestione dei sedimenti alluvionali dell'alveo del fiume Po – Stralcio confluenza Arda, incile Po di Goro: deliberazione n. 1 del Comitato Istituzionale del 24 gennaio 2008, Parma. 262 p. In Italian.

AdBPo., 2008d. Autorità di Bacino Distrettuale del Fiume Po, Stralcio "di monte" Programma generale di gestione dei sedimenti alluvionali dell'alveo del fiume Po – Stralcio confluenza Stura di Lanzo, confluenza Tanaro: deliberazione n. 3 del Comitato Istituzionale del 18 marzo 2008, Parma. 100 p. In Italian.

Amadori, C., Toscani, G., Di Giulio, A., Maesano, F.E., D'Ambrogi, C., Ghielmi, M., Fantoni, R., 2019. From cylindrical to non-cylindrical foreland basin: Pliocene–Pleistocene evolution of the Po Plain–Northern Adriatic basin (Italy). Basin Res. 31 (5), 991–1015. https://doi.org/10.1111/bre.12369.

Amorosi, A., Milli, S., 2001. Late quaternary depositional architecture of Po and Tevere River deltas (Italy) and worldwide comparison with coeval deltaic successions. Sediment. Geol., 144, 357–375. https://doi.org/10.1016/S0037-0738(01)00129-4.

Arpa Lombardia, 2024. Database precipitazione della Regione Lombardia. https://idro.arpalombardia.it/it/map/sidro/ (accessed 02 September 2024).

Arpa Piemonte, 2024. Database precipitazione della Regione Piemonte. https://www.arpa.piemonte.it/rischi_naturali/snippets_arpa_graphs/map_meteoweb/?rete=stazione_centenaria (accessed 02 September 2024).

Arpae Emilia-Romagna, 2017. Rapporto IdroMeteoClima Emilia-Romagna, 2017, 63 p. https://www.arpae.it/it/temi-ambientali/meteo/report-meteo/rapporti-annuali (accessed 02 September 2024).

Arpae Emilia-Romagna, 2021. Rapporto IdroMeteoClima Emilia-Romagna, 2021, 69 p. https://www.arpae.it/it/temi-ambientali/meteo/report-meteo/rapporti-annuali (accessed 03 September 2024).

Arpae Emilia-Romagna, 2023. Rapporto IdroMeteoClima Emilia-Romagna, 2023, 100 p. https://www.arpae.it/it/temi-ambientali/meteo/report-meteo/rapporti-annuali (accessed 03 September 2024).

Belletti, B., Nardi, L., Rinaldi, M., 2016. Diagnosing problems induced by past gravel mining and other disturbances in Southern European rivers: the Magra River, Italy. Aquatic Science. 78, 107–119. https://doi.org/10.1007/s00027-015-0440-5.

Belletti, B., Garcia de Leaniz, C., Jones, J., et al., 2020. More than one million barriers fragment Europe's rivers. Nature 588, 436–441. https://doi.org/10.1038/s41586-020-3005-2.

Bertrand, M., Liébault, F., 2019. Active channel width as a proxy of sediment supply from mining sites in New Caledonia: Earth Surface Processes and Landforms. 44, 67–76, https://doi.org/10.1002/esp.4478.

Bollati, I.M., Pellegrini, L., Rinaldi, M., Duci, G., Pelfini, M., 2014. Reach-scale morphological adjustments and stages of channel evolution: the case of the Trebbia River (northern Italy). Geomorphology 221, 176–186. https://doi.org/10.1016/j.geomorph.2014.06.007.

Brenna, A., Bizzi, S., Surian, N., 2024. How multiple anthropic pressures may lead to unplanned channel patterns: insights from the evolutionary trajectory of the Po River (Italy). Catena 234, 107598. https://doi.org/10.1016/j.catena.2023.107598.

Brierley, G.J., Hikuroa, D., Fuller, I.C., Tunnicliffe, J., Allen, K., Brasington, J., Friedrich, H., Hoyle, J., Measures, R., 2023. Reanimating the strangled rivers of Aotearoa New Zealand. WIREs Water 10 (2), e1624. https://doi.org/10.1002/wat2.1624.

Brunsden, D., 1993. Barriers to geomorphological change. In: Thomas, D.S.G., Allison, R. J. (Eds.), Landscape Sensitivity. John Wiley & Sons, Chichester, pp. 7–12.

Brunsden, D., Thornes, J.B., 1979. Landscape sensitivity and change: Transactions of the Institute of British Geographers. 4, 463–484. https://doi.org/10.2307/622210.

Carbonneau, P.E., Dugdale, S.J., Breckon, T.P., Dietrich, J.T., Fonstad, M.A., Miyamoto, H., Woodget, A.S., 2020. Adopting deep learning methods for airborne rgb fluvial scene classification. Remote Sens. Environ. 251.

Carminati, E., Doglioni, C., 2012. Alps vs. Apennines: The paradigm of a tectonically asymmetric Earth. Earth Sci. Rev. 112 (1-2), 67–96. https://doi.org/10.1016/j.earscirev. 2012.02.004.

Castiglioni, G.B., Biancotti, A., Bondesan, M., Cortemiglia, G.C., Elmi, C., Favero, V., et al., 1999. Geomorphological map of the Po plain, Italy, at a scale of 1: 250 000. Earth Surf. Proc. Land. 24 (12), 1115–1120. https://doi.org/10.1002/(SICI)1096-9837(199911)24:12<1115:AID-ESP38>3.0.CO;2.

Cattaneo, A., Correggiari, A., Langone, L., et al., 2003. The late-Holocene Gargano subaqueous delta, Adriatic shelf: sediment pathways and supply fluctuations. Mar. Geol. 193, 61–91. https://doi.org/10.1016/S0025-3227(02)00614-X.

Church, M., 2006. Bed material transport and the morphology of alluvial river channels: Annual Review of Earth and Planetary Sciences. 34(1), 325–354. https://doi.org/10.1146/annurev.earth.33.092203.122721.

Clerici, A., Perego, S., Chelli, A., Tellini, C., 2015. Morphological changes of the floodplain reach of the Taro River (Northern Italy) in the last two centuries. J. Hydrol. 527, 1106–1122. https://doi.org/10.1016/j.jhydrol.2015.05.063.

Comiti, F., 2012. How natural are Alpine mountain rivers? Evidence from the Italian Alps. Geomorphology 37, 693–707. https://doi.org/10.1002/esp.2267.

Cook, K.L., Turowski, J.M., Hovius, N., 2020. Width control on event-scale deposition and evacuation of sediment in bedrock-confined channels: Earth Surface Processes and Landforms. 45 (14), 3702–3713. https://doi.org/10.1002/esp.4993.

Coward, M. P., Dietrich, D., Park, R. G., 1989. Alpine Tectonics. Geological Society of London, Special Publications. 45, 449. https://doi.org/10.1017/S0016756800015302.

David, M., Labenne, A., Carozza, J.M., Valette, P., 2016. Evolutionary trajectory of channel planforms in the middle Garonne River (Toulouse, SW France) over a 130-year period: Contribution of mixed multiple factor analysis (MFAmix). Geomorphology 258, 21–39. https://doi.org/10.1016/j.geomorph.2016.01.012.

Diodato, N., Ljungqvist, F.C., Bellocchi, G., 2020. Monthly storminess over the Po River Basin during the past millennium (800–2018 CE). Environ. Res. Commun. 2 (3), 031004. https://doi.org/10.1088/2515-7620/ab7ee9.

Doglioni, C., 1993. Some remarks on the origin of foredeeps. Tectonophysics 288, 1–20. https://doi.org/10.1016/0040-1951(93)90211-2.

Domeneghetti, A., Carisi, F., Castellarin, A., Brath, A., 2015. Evolution of flood risk over large areas: Quantitative assessment for the Po river. J. Hydrol. 527, 809–823. https://doi.org/10.1016/j.jhydrol.2015.05.043.

Dunne, T., Mertes, L.A.K., Meade, R.H., Richey, J.E., Forsberg, B.R., 1998. Exchanges of sediment between the flood plain and channel of the Amazon River in Brazil: Geological Society of America Bulletin. 110, 450–467. https://doi .org/10.1130/0016-7606(1998)110<0450:EOSBTF>2 .3.CO;2.

Fantoni, R., Franciosi, R., 2010. Tectono-sedimentary setting of the Po Plain and Adriatic foreland. Rendiconti Lincei. 21 (1), 197–209. https://doi.org/10.1007/s12210-010-0102-4.

Ferguson, R.I., 1986. Hydraulics and hydraulic geometry. Prog. Phys. Geogr. 10, 1–31. https://doi.org/10.1177/030913338601000101.

Frissell, C.A., Liss, W.L., Warren, C.E., Hurley, M.D., 1986. A hierarchical framework for stream habitat classification: viewing streams in a watershed context. Environ. Manag. 10, 199–214. https://doi.org/10.1007/BF01867358.

Fryirs, K.A., Wheaton, J.M., Brierley, G.J., 2016. An approach for measuring confinement and assessing the influence of valley setting on river forms and processes. Earth Surf. Proc. Land. 41, 701–710. https://doi.org/10.1002/esp.3893.
Galvani, I., Pellegrini, M., 2009. Navigare il Po, tra passato e futuro. In: Ferrari, I., Pellegrini, M. (Eds.), Un Po Di Carte. La Dinamica Fluviale Dell'ottocento e Le Tavole Della Commissione Brioschi. Ed. Diabasis. Reggio Emilia, pp. 51–65.
Garzanti, E., Vezzoli, G., Andò, S., 2011. Paleogeographic and paleodrainage changes during Pleistocene glaciations (Po Plain, northern Italy). Earth Sci. Rev. 105 (1–2), 25–48. https://doi.org/10.1016/j.earscirev.2010.11.004.
Garzanti, E., Resentini, A., Vezzoli, G., Andò, S., Malusà, M., Padoan, M., 2012. Forward compositional modelling of Alpine orogenic sediments. Sediment. Geol. 280, 149–164. https://doi.org/10.1016/j.sedgeo.2012.03.012.
Garzanti, E., Wang, J.G., Vezzoli, G., Limonta, M., 2016. Tracing provenance and sediment fluxes in the Irrawaddy River basin (Myanmar). Chem. Geol. 440, 73–90. https://doi.org/10.1016/j.chemgeo.2016.06.010.
Ghielmi, M., Minervini, M., Nini, C., Rogledi, S., Rossi, M., 2013. Late Miocene-Middle Pleistocene sequences in the Po Plain-Northern Adriatic Sea (Italy): The stratigraphic record of modi- fication phases affecting a complex foreland basin. Mar. Pet. Geol. 42, 50–81. https://doi.org/10.1016/j.marpetgeo.2012.11.007.
Gilbert, G.K., 1914. The Transportation of Debris by Running Water: U.S. Geological Survey Professional Paper. 86, 263 p. https://doi.org/10.5962/bhl.title.45583.
Gorio, O., 1954. Ventidue anni di studi e lavori sul Po dal 1919 al 1941. Cartotecnica Romana, Roma (Italy). In Italian.
Grant, G.E., 2012. The geomorphic response of gravel-bed rivers to dams: perspectives and prospects. In: Church, M., Biron, P., Roy, A. (Eds.), Gravel Bed Rivers: Processes, Tools, Environments. John Wiley & Sons Ltd, pp. 165–181.
Grant, G.E., O'Connor, J., Safran, E., 2017. Excursions in river (dis)continuity. Geomorphology 277, 145–153.
Hassan, M.A., Smith, B.J., Hogan, D.L., Luzi, D.S., Zimmermann, A.E., Eaton, B.C., 2007. Sediment storage and transport in coarse bed streams: Scale considerations. Gravel Bed Rivers. 7 (11), 473–496. https://doi.org/10.1016/S0928-2025(07)11137-8.
Hassan, M.A., Pierce, J.K., Chartrand, S.M., 2024. Sediment storage and fluvial sediment transport linkages across an experimental flood sequence. J. Geophys. Res. Earth 129, e2024JF007772. https://doi.org/10.1029/2024JF007772.
IDROSER (Idrorisorse per lo sviluppo dell'Emilia-Romagna), 1981. Piano progettuale per la difesa della costa adriatica Emiliano-Romagnola: Bologna, Idroser, il Trasporto Solido Fluviale nei Bacini Tributari dell'Adriatico. 4, 429 p.
Keesstra, S.D., van Huissteden, J., Vandenberghe, J., Van Dam, O., de Gier, J., Pleizer, I. D., 2005. Evolution of the morphology of the river Dragonja (SW Slovenia) due to land-use changes. Geomorphology 69, 191–207. https://doi.org/10.1016/j.geomorph.2005.01.004.
Kellerhals, R., Church, M., 1989. The Morphology of Large Rivers: Characterization and Management. In: Dodge, D.P. (Ed.), Proceedings of the International Large River Symposium, Canadian Special Publication of Fisheries and Aquatic Sciences, pp. 31–48.
Latapie, A., Camenen, B., Rodrigues, S., Paquier, A., Bouchard, J.P., Moatar, F., 2014. Assessing channel response of a long river influenced by human disturbance. Catena 121, 1–12. https://doi.org/10.1016/j.catena.2014.04.017.
Leopold, L.B., Maddock, T., 1953. The hydraulic geometry of stream channels and some physiographic implications. Professional Paper 252, USGS, Washington D.C., 57 p.
Leopold, L.B., Bull, W.B., 1979. Base level, aggradation, and grade. Proc. Am. Philos. Soc. 123 (2), 168–202.
Leopold, L.B., Wolman, M.G., Miller, J.P., 1964. Fluvial processes in geomorphology. W. H. Freeman and Company, San Francisco.
Liébault, F., Piégay, H., 2001. Assessment of channel changes due to long-term bedload supply decrease, Roubion River, France. Geomorphology. 36, 167–186. https://doi.org/10.1016/S0169-555X(00)00044-1.
Liébault, F., Piégay, H., 2002. Causes of 20th century channel narrowing in mountain and piedmont rivers of Southeastern France. Earth Surf. Proc. Land. 27, 425–444. https://doi.org/10.1002/esp.328.
Lisle, T.E., 1982. Effects of aggradation and degradation on riffle-pool morphology in natural gravel channels, northwestern California. Water Resour. Res. 18 (6), 1643–1651. https://doi.org/10.1029/WR018i006p01643.
Livani, M., Petracchini, L., Benetatos, C., Marzano, F., Billi, A., Carminati, E., Doglioni, C., Petricca, P., Maffucci, R., Codegone, G., Rocca, V., 2023. Subsurface geological and geophysical data from the Po Plain and the northern Adriatic Sea (north Italy). Earth Syst. Sci. Data Discuss. 15, 4261–4293. https://doi.org/10.5194/essd-15-4261-2023.
Llena, M., Vericat, D., Martínez-Casasnovas, J.A., Smith, M.W., 2020. Geomorphic adjustments to multiscale disturbances in a mountain river: A century of observations. Catena 192. https://doi.org/10.1016/j.catena.2020.104584.
Llena, M., Simonelli, T., Brardinoni, F., 2024. Inherited anthropogenic disturbance and decadal sediment dynamics in a mountain fluvial system: the case of the Marecchia River canyon, Northern Apennines. Geol. Soc. Am. Bull. 136, 741–764. https://doi.org/10.1130/B36720.1.
Luzi, D., Hassan, M.A., Papangelakis, E., Eaton, E., 2021. Cycles of aggradation and degradation in Gravel-bed Rivers mediated by sediment storage and morphologic evolution. Geomorphology 395, 108001. https://doi.org/10.1016/j.geomorph.2021. 108001.
Mackin, J.H., 1948. Concept of the Gravel River: Geological Society of America Bulletin. 59, 463–512. https:// doi.org/10.1130/0016-7606(1948)59[463:COTGR]2.0.CO;2.
Madej, M.A., 2001. Development of channel organization and roughness following sediment pulses in single-thread, gravel bed rivers. Water Resour. Res. 37 (8), 2259–2272. https://doi.org/10.1029/2001WR000229.
Magdaleno, F., Anastasio Fernández, J., Merino, S., 2012. The Ebro River in the 20th century or the ecomorphological transformation of a large and dynamic Mediterranean channel. Earth Surf. Proc. Land. 37 (5), 486–498. https://doi.org/10.1002/esp.2258.
MagisPo, 1954. Magistrato per il Po – Ministero dei lavori pubblici. Carta tecnica del Fiume Po, scala 1:10.000, edizione 1954. http://geoportale.agenziapo.it/web/index.php/it/ (accessed February 2024).
MagisPo, 1979. Magistrato per il Po – Ministero dei lavori pubblici. Carta tecnica del Fiume Po, scala 1:10.000, edizione 1979. http://geoportale.agenziapo.it/web/index.php/it/ (accessed March 2024).
Mandarino, A., Maerker, M., Firpo, M., 2019. Channel planform changes along the Scrivia River floodplain reach in northwest Italy from 1878 to 2016. Quat. Res. 91 (2), 620–637. https://doi.org/10.1017/qua.2018.67.
Marchetti, M., 2002. Environmental changes in the central Po Plain (northern Italy) due to fluvial modifications and anthropogenic activities. Geomorphology 44 (3–4), 361–373. https://doi.org/10.1016/S0169-555X(01)00183-0.
Marchi, E., Roth, G., Siccardi, F., 1995. The November 1994 flood event on the Po River: structural and non-structural measures against inundations, in Workshop on the hydrometeorology, impacts, and Management of Extreme Floods. Perugia (Italy) 1–28.
Maselli, V., Pellegrini, C., del Bianco, F., Mercorella, A., Nones, M., Crose, L., et al., 2018. River morphodynamic evolution under dam-induced backwater: an example from the Po River (Italy). J. Sediment. Res. 88 (10), 1190–1204. https://doi.org/10.2110/jsr.2018.61.
Mason, R.J., Johnson, M.F., Wohl, E., Russell, C.E., Olden, J.D., Polvi, L.E., et al., 2025. Rebalancing River Lateral Connectivity: An Interdisciplinary Focus for Research and Management. Wiley Interdiscip. Rev. Water 12 (1), e1766.
Montanari, A., 2012. Hydrology of the Po River: looking for changing patterns in river discharge. Hydrol. Earth Syst. Sci. 16, 3739–3747. https://doi.org/10.5194/hess-16-3739-2012.
Montanari, A., Nguyen, H., Rubinetti, S., Ceola, S., Galelli, S., Rubino, A., Zanchettin, D., 2023. Why the 2022 Po River drought is the worst in the past two centuries. Sci. Adv. 9 (32), eadg8304. https://doi.org/10.1126/sciadv.adg8304.
Montgomery, D.R., Buffington, J.M., 1997. Channel-reach morphology in mountain drainage basins. Geol. Soc. Am. Bull. 109, 596–611. https://doi.org/10.1130/0016-7606(1997)109<0596:CRMIMD>2.3.CO;2.
Muttoni, G., Carcano, C., Garzanti, E., Ghielmi, M., Piccin, A., Pini, R., Rogledi, S., Sciunnach, D., 2003. Onset of major Pleistocene glaciations in the Alps. Geology 31, 989–992. https://doi.org/10.1130/G19445.1.
NIER/CER, 1982. Indagine fotointerpretativa dell'alveo del Fiume Po dalla confluenza del Tanaro a Pontelagoscuro. Studio Geologico GEOMAP di Firenze.
Nones, M., Guerrero, M., Schippa, L., Cavalieri, I., 2024. Remote sensing assessment of anthropogenic and climate variation effects on river channel morphology and vegetation: Impact of dry periods on a European piedmont river. Earth Surf. Proc. Land. 49 (5), 1632–1652. https://doi.org/10.1002/esp.5791.
O'Brien, G.R., Wheaton, J.M., Fryirs, K., Macfarlane,W .W., Brierley, G., Whitehead, K., Gilbert, J., Volk, C., 2019, Mapping valley bottom confinement at the network scale: Earth Surface Processes and Landforms. 44, 1828–1845, https://doi.org/10.1002/esp.4615.
Ollero, A., 2010. Channel changes and floodplain management in the meandering middle Ebro River, Spain. Geomorphology. 117, 247–260. https://doi.org/10.1016/j.geomorph.2009. 01.015.
Ori, G.G., 1993. Continental depositional systems of the Quaternary of the Po Plain (northern Italy). Sediment. Geol. 83, 1–143. https://doi.org/10.1016/S0037-0738(10)80001-6.
Parrinello, G., Bizzi, S., Surian, N., 2021. The retreat of the delta: a geomorphological history of the Po River basin during the twentieth century. Water Hist. 13, 1–20. https://doi.org/10.1007/s12685-021-00279-3.
Pellegrini, L., Maraga, F., Turitto, O., Audisio, C., Duci, G., 2008. Evoluzione morfologica di alvei fluviali mobili nel settore occidentale del bacino padano. Italian J. Quat. Sci. 21, 251–266.
Persichillo, M.G., Bordoni, M., Meisina, C., 2017. The role of land use changes in the distribution of shallow landslides. Sci. Total Environ. 574, 924–937. https://doi.org/10.1016/j.scitotenv.2016.09.125.
Persichillo, M.G., Bordoni, M., Cavalli, M., Crema, S., Meisina, C., 2018. The role of human activities on sediment connectivity of shallow landslides. Catena 160, 261–274. https://doi.org/10.1016/j.catena.2017.09.025.
Pieri, M., Groppi, G., 1981. Subsurface geological structure of the Po Plain, Italy. Progetto Finalizzato Geodin. 414, 1–13.
Pittau, S., Rossi, M., Llena, M., Brardinoni, F., 2024. Evaluating historical, basin-wide landslide activity in a context of land abandonment and climate change: Effects of landslide visibility and temporal resolution. Geomorphology 452, 109122. https://doi.org/10.1016/j. geomorph.2024.109122.
Provansal, M., Dufour, S., Sabatier, F., Anthony, E., Raccasi, G., Robresco, S., 2014. The geomorphic evolution and sediment balance of the lower Rhône River (southern France) over the last 130 years: hydropower dams versus other control factors. Geomorphology 219, 27. https://doi.org/10.1016/j.geomorph.2014.04.033.
Pryor, B.S., Lisle, T., Montoya, D.S., Hilton, S., 2011. Transport and storage of bed material in a gravel-bed channel during episodes of aggradation and degradation: A field and flume study. Earth Surf. Proc. Land. 36 (15), 2028–2041. https://doi.org/10.1002/esp.2224.
Rascher, E., Rindler, R., Habersack, H., Sass, O., 2018. Impacts of gravel mining and renaturation measures on the sediment flux and budget in an alpine catchment (Johnsbach Valley, Austria): Geomorphology. 318, 404-420. https://doi.org/10.1016/j.geomorph.2018.07.009.
Rinaldi, M., 2021. Bed-level adjustments in the Po River catchment (Northern Italy). Italian J. Eng. Geology Environ. 2, 41–50.

Rinaldi, M., Teruggi, L.B., Simoncini, C., Nardi, L., 2008. Dinamica recente ed attuale di alvei fluviali: alcuni casi di studio dell'Appennino Settentrionale. Alpine and Mediterranean Quaternary 21 (1B), 291–302.

Rinaldi, M., Surian, N., Pellegrini, L., Maraga, F., Turitto, O., 2010. Attuali conoscenze sull'evoluzione recente di corsi d'acqua del Bacino Padano ed implicazioni per la gestione e riqualificazione fluviale. Biologia Ambientale 24 (1), 29–40.

Scardia, G., Franco, R., Muttoni, G., Rogledi, S., Caielli, G., Carcano, C., Sciunnach, D., Piccin, A., 2012. Stratigraphic evidence of a Middle Pleistocene climate-driven flexural uplift in the Alps. Tectonics 31 (6), 2012TC003108. https://doi.org/10.1029/2012TC003108.

Schumm, S.A., 1977. The Fluvial System. Wiley, New York, p. 338.

Schumm, S.A., 1985. Patterns of alluvial rivers. Annu. Rev. Earth Planet. Sci. 13, 5–27. https://doi.org/10.1146/annurev.ea.13.050185.000253.

Scorpio, V., Comiti, F., Liébault, F., Piegay, H., Rinaldi, M., Surian, N., 2024. Channel changes over the last 200 years: A meta data analysis on European rivers. Earth Surf. Proc. Land. 49 (9), 2651–2676. https://doi.org/10.1002/esp.5848.

Scorpio, V., Piégay, H., 2021. Is afforestation a driver of change in Italian rivers within the Anthropocene era? Catena 198, 105031. https://doi.org/10.1016/j.catena.2020.105031.

Surian, N., Rinaldi, M., 2003. Morphological response to river engineering and management in alluvial channels in Italy. Geomorphology 50 (4), 307–326. https://doi.org/10.1016/S0169-555X(02)00219-2.

Surian, N., Rinaldi, M., Pellegrini, L., Audisio, C., Maraga, F., Teruggi, L., et al., 2009. Channel adjustments in northern and central Italy over the last 200 years. In: James, L.A., Rathburn, S.L., Whittecar, G.R. (Eds.), Management and Restoration of Fluvial Systems with Broad Historical Changes and Human Impacts: Geological Society of America Special Paper, pp. 83–95. https://doi.org/10.1130/2009.2451(05).

Wheaton, J.M., Brasington, J., Darby, S.E., Sear, D.A., 2010.Accounting for uncertainty in DEMs from repeat topographic surveys: Improved sediment budgets: Earth Surface Processes and Landforms. 35 (2), 136–156. https://doi.org/10.1002/esp.1886.

Wieland, M., Martinis, S., Kiefl, R., Gstaiger, V., 2023. Semantic segmentation of water bodies in very high-resolution satellite and aerial images. Remote Sensing of Environment 287, 113452. https://doi.org/10.1016/j.rse.2023.113452.

Ylla Arbós, C., Blom, A., Viparelli, E., Reneerkens, M., Frings, R.M., Schielen, R.M.J., 2021. River response to anthropogenic modification: Channel steepening and gravel front fading in an incising river. Geophys. Res. Lett. 48, e2020GL091338. https://doi.org/10.1029/2020GL091338.

Zanchettin, D., Traverso, P., Tomasino, M., 2008. Po River discharge: a preliminary analysis of a 200-year time series. Clim. Change. 88, 411–433. https://doi.org/10.1007/s10584-008-9395-z.